the neural and peripheral arcs, the maximal gains (at the mid-point of the arc) and operating gains (at the intersection of arcs) were similar in supine and upright tilt positions. All parameters (P_{1-4}) and the maximal gain of the total arc were similar in supine and upright tilt positions (Table 3).

Using the data from all animals, the operating AP estimated from the baroreflex open-loop equilibrium diagram (protocols 1 and 3) agreed with those measured in the baroreflex closed-loop condition (protocol 2) for both postures (Fig. 6*A*). The operating SNA values estimated from the equilibrium diagram also agreed with those measured for both postures (Fig. 6*B*).

Discussion

The maintenance of AP in upright posture against gravitational fluid shift is of great importance, but the mechanisms remain unknown. We applied baroreflex equilibrium diagram analysis (Yamamoto *et al.* 2004) to the baroreflex system both in supine and 60 deg upright tilt positions. Our new major findings are that upright tilt shifts the CSP–SNA relationship (the baroreflex neural arc) to a higher SNA, whereas it shifts the SNA–AP relationship (the baroreflex peripheral arc) to a lower AP (Fig. 5). These data support our first hypothesis that orthostatic stress resets the baroreflex neural arc to a higher SNA.

Our data indicate that resetting of the baroreflex neural arc in an upright posture doubles the orthostatic activation of SNA and increases the operating AP by 10 mmHg. In our experiments, 60 deg upright tilt reset the neural arc to a higher SNA, shifted the peripheral arc to a lower AP (Fig. 5*A* and *B*), and consequently moved the estimated operating point from point S (SNA, 66 a.u.; AP, 102 mmHg) to point U at a higher SNA (91 a.u) and similar AP (102 mmHg) (Fig. 5*C*). In a simulation where the resetting in the neural arc is absent, 60 deg upright tilt would move the operating point from point S to point A (the intersection of the supine neural arc and the upright-tilt peripheral arc: SNA, 79 a.u.; AP, 92 mmHg),

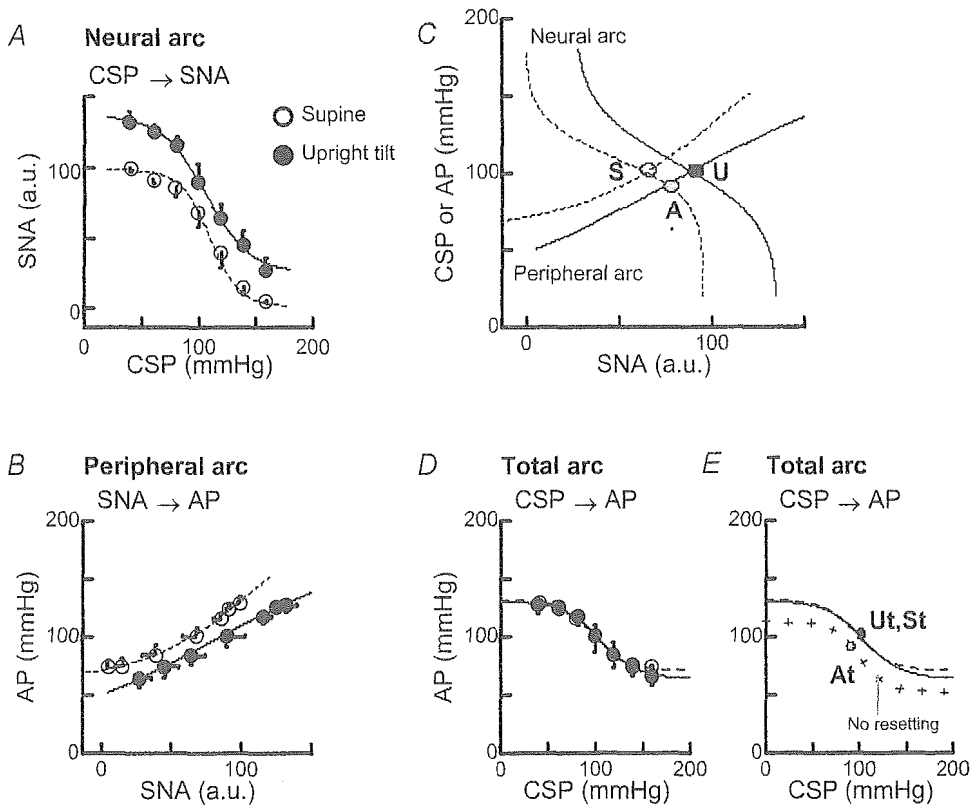

Figure 5. Baroreflex neural arc (*A*), peripheral arc (*B*) and total arc (*D* and *E*) and the baroreflex equilibrium diagram (*C*) in supine (○, dotted line) and 60 deg upright tilt positions (●, continuous line)
Data were averaged from all animals ($n = 8$) and presented as means ± S.D. Dotted and continuous lines are four-parameter logistic functions fitted to the averaged data. In the baroreflex equilibrium diagram (*C*), point S and U indicate the estimated operating points in supine and upright tilt positions, respectively. Point A (grey circle) indicates the estimated operating point in upright tilt position in the absence of neural arc shift (*C*). In the total arc (*E*), points St and Ut indicate the estimated operating points in supine and upright tilt positions, respectively. The two points are superimposed. The line joining the crosses and point At (grey circle) indicate the estimated total arc curve and operating point, respectively, in the absence of neural arc shift (simulation) (*E*).

Table 1. The operating points estimated from equilibrium diagram

	Supine	Upright tilt	Simulated upright tilt without resetting of the neural arc
AP (mmHg)	102 ± 4	102 ± 4	92 ± 3*†
SNA (a.u)	66 ± 6	91 ± 5*	79 ± 5*†

Values are means ± S.D. ($n = 8$). *$P < 0.05$ *versus* Supine. †$P < 0.05$ Upright tilt *versus* Simulated upright tilt without resetting of the neural arc.

Table 2. Effect of upright tilt on the baroreflex neural and peripheral arc parameters

	Supine	Upright tilt
Neural arc		
P_1 (a.u.)	94 ± 2	112 ± 5*
P_2 (a.u. mmHg^{-1})	0.10 ± 0.01	0.09 ± 0.02
P_3 (mmHg)	109 ± 6	109 ± 6
P_4 (a.u.)	4 ± 1	29 ± 6*
G_{max} (a.u. mmHg^{-1})	−2.5 ± 0.4	−2.3 ± 0.4
Peripheral arc		
P_1 (mmHg)	115 ± 18	82 ± 12*
P_2 (mmHg a.u.$^{-1}$)	−0.04 ± 0.01	−0.05 ± 0.01
P_3 (a.u.)	63 ± 8	88 ± 7*
P_4 (mmHg)	50 ± 9	50 ± 5
G_{max} (mmHg a.u.$^{-1}$)	1.2 ± 0.4	1.0 ± 0.1

Values are means ± S.D. ($n = 8$). See eqn (1) in Methods for definition of the four parameters of the logistic function. *$P < 0.05$, Supine *versus* Upright tilt.

Table 3. Effect of upright tilt on the baroreflex total arc parameters

	Supine	Upright tilt
P_1 (mmHg)	61 ± 4	67 ± 4
P_2	0.05 ± 0.01	0.05 ± 0.02
P_3 (mmHg)	98 ± 6	103 ± 6
P_4 (mmHg)	70 ± 4	65 ± 4
G_{max}	−0.8 ± 0.2	−0.8 ± 0.2

Values are means ± S.D. ($n = 8$). See eqn (1) in Methods for definition of the four parameters of the logistic function. All parameters were similar in supine and upright tilt positions.

halving the orthostatic activation of SNA (13 a.u. *versus* 25 a.u) and decreasing the operating AP at upright tilt by 10 mmHg compared with when the resetting is in operation. These findings support our second hypothesis that resetting of the arterial baroreflex contributes to preventing postural hypotension.

Our data indicate that resetting of the baroreflex neural arc contributes to preserving the baroreflex total arc function in an upright posture. In a simulation where resetting in the neural arc is absent, 60 deg upright tilt would shift the total arc downward to a lower AP (Fig. 5*D* and *E*) by a downward shift of the peripheral arc. However, in our experiments, 60 deg upright tilt maintained the total arc (Fig. 5*D* and *E*) by orthostatic resetting of the neural arc. These findings indicate that resetting of the neural arc has an important role in maintaining the total baroreflex function in an upright posture.

Little is known about the arterial baroreflex system under orthostatic stress. Although earlier studies addressed the baroreflex in relation to AP regulation under orthostatic stress, most of them evaluated the baroreflex in a supine, not orthostatic, position (Mosqueda-Garcia *et al.* 1997). In addition, although earlier studies investigated the gains of baroreflex control of SNA (Mosqueda-Garcia *et al.* 1997), vascular resistance (Cooper & Hainsworth, 2001) and R–R interval (Cooke *et al.* 1999), these gains were part of the total baroreflex system, and thus could not explain the operating points of the baroreflex. In the present study, we determined the neural and peripheral arcs independently in an upright position using the baroreflex open-loop equilibrium diagram. We found that upright tilt shifted the baroreflex neural arc to a higher SNA, while it shifted the baroreflex peripheral arc to a lower AP. Our data confirmed the accuracy of the equilibrium diagram in defining the operating point, since in both supine and upright tilt positions, the operating points estimated from the diagram agreed well with those measured in the baroreflex closed-loop condition (Fig. 6). This is consistent with earlier studies addressing haemorrhage (Sato *et al.* 1999) and muscle stretch (Yamamoto *et al.* 2004).

The mechanism responsible for the resetting of baroreflex neural arc with upright tilt remains unclear. The most likely mechanism is recruitment of other sympathoexcitatory systems than the baroreflex during orthostatic stress. In particular, the vestibular system is stimulated by upright tilt, and has been reported to increase SNA (vestibulosympathetic reflex) (Yates, 1992) and assist AP regulation during orthostatic stress in humans (Ray & Carter, 2003) and rats (Gotoh *et al.* 2004). In addition, contractions of the antigravity muscles during upright tilt stimulate the muscle reflexes that increase SNA (Potts & Mitchell, 1998; Yamamoto *et al.* 2004). Thus recruitments of other systems may shift the CSP–SNA relationship to a higher SNA.

However, the resetting of the baroreflex neural arc during upright tilt may not result from simple summation of SNA activation by the arterial baroreflex and by other systems. Theoretically, if the recruitments of other systems only offset SNA, it increases P_4 (the minimum value of SNA) but not P_1 (the range of SNA response to CSP) of the neural arc, and causes a parallel shift of the CSP–SNA relationship to a higher SNA without transforming the inverse sigmoid curve. In contrast, our results showed that 60 deg upright tilt increased not only P_4 but also P_1 (Table 2), and widened the inverse sigmoid curve. These findings suggest an interaction between baroreflex and

other systems in upright tilt posture. Indeed, the vestibular system has been considered to interact with the baroreflex (Yates, 1992; Kaufmann *et al.* 2002; Monahan & Ray, 2002; Ray & Carter, 2003; Gotoh *et al.* 2004). In addition, the muscle reflex has been reported to interact with the baroreflex (Potts & Mitchell, 1998), and contribute to the central resetting of the baroreflex during exercise (DiCarlo & Bishop, 2001; Miki *et al.* 2003). We have recently reported that passive stretch of the triceps surae muscles shifts the CSP–SNA relationship to a higher SNA using the baroreflex equilibrium diagram analysis (Yamamoto *et al.* 2004). Further studies are necessary to address the mechanism for the resetting during upright tilt.

Our data indicate that 60 deg upright tilt reduces the pressor response to SNA in the peripheral cardiovascular system. We observed that upright tilt down-shifted the baroreflex peripheral arc to a lower AP. For all SNA levels, AP was lower in the upright than supine position (Figs 4 and 5). This change may be attributed to the gravitational fluid shift toward the lower part of the body (i.e. abdominal vascular bed, lower limbs), which decreases the preload and effective circulatory blood volume (Sagawa *et al.* 1988; Rowell, 1993).

Our data suggest that upright tilt yields a different effect on the baroreflex system compared with haemorrhage. Haemorrhage decreases effective circulatory blood volume and preload (Sagawa *et al.* 1988; Rowell, 1993). Earlier study in rats demonstrated that haemorrhage (blood loss in the range of 0.5–2% of body weight) reduced AP in a prevailing level of SNA in the baroreflex peripheral arc (Sato *et al.* 1999), similar to our upright tilt. Therefore, both upright tilt and haemorrhage reduce the pressor response to SNA in the peripheral cardiovascular system. In contrast to upright tilt, haemorrhage did not affect the baroreflex neural arc (Sato *et al.* 1999). In short, upright tilt resets the baroreflex neural arc to a higher SNA whereas haemorrhage does not.

Since we focused on arterial baroreflex dynamics in response to an acute orthostatic stress, our findings could not relate long-term pressure regulation by arterial and cardiopulmonary baroreflexes and the renin–angiotensin system. Early study showed that chronic sino-aortic and cardiopulmonary denervations increased AP and activated the renin–angiotensin system in the conscious dog (Persson *et al.* 1988). Further study is needed to address long-term orthostatic physiology.

As we investigated the role of the arterial baroreflex in AP control under orthostatic stress while AP was well maintained, our findings could not explain the pathophysiology of orthostatic vasovagal syncope. Interestingly, the final trigger of human orthostatic syncope appears to be the abrupt disappearance of SNA (Morillo *et al.* 1997). Given the present findings, we speculate that some changes in the baroreflex neural arc can decrease SNA and trigger orthostatic syncope.

Limitations

The present study has several limitations. First, we excluded the efferent effect of vagally mediated arterial baroreflex, which could affect the properties of the two arcs. Second, we used an anaesthetic agent (intravenous injection of a mixture of urethane and α-chloralose) that could flatten the baroreflex peripheral arc by reducing the cardiac pumping function.

Third, since we measured only renal SNA, our findings have limited applicability to other SNA, including cardiac SNA. Although static regulation of the baroreflex neural arc over SNA is similar in renal and cardiac SNAs in

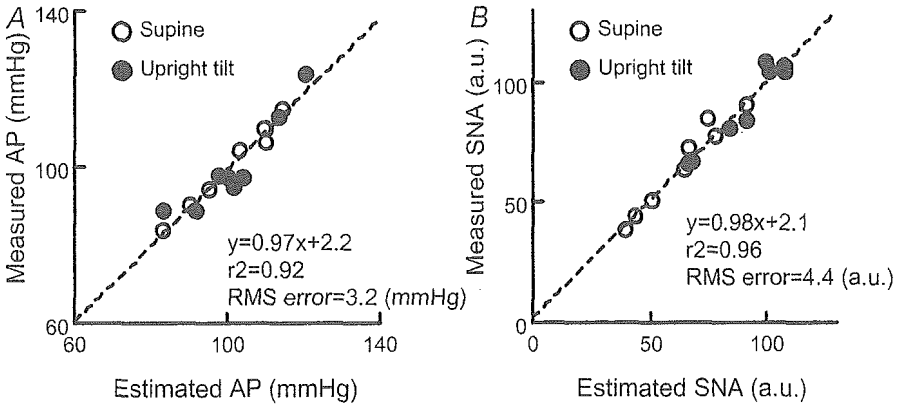

Figure 6. The relationship between the operating points estimated from the baroreflex open-loop equilibrium diagram (protocols 1 and 3) and those actually measured under the baroreflex closed-loop condition (protocol 2) in all animals ($n = 8$)

A and *B* show the operating AP and SNA, respectively. Each animal provided two data points obtained in supine (open circles) and upright tilt positions (filled circles). Both the operating AP and SNA estimated by the equilibrium diagram match the values actually measured under the baroreflex closed-loop condition. RMS: root mean square.

supine posture (Kawada *et al.* 2001), whether this holds true during orthostatic stress remains to be verified.

Fourth, we were not able to quantify the contribution of cardiac function (i.e. cardiac output) to AP regulation. Since the baroreflex peripheral arc represents the static relation from SNA input to AP, it includes the effects of SNA on cardiac function, stressed blood volume and vascular resistance. We were not able to isolate these factors because of complexity and experimental difficulties.

Fifth, we eliminated cardiopulmonary baroreflex by cutting bilateral vagal nerves. Earlier human studies have indicated that non-hypotensive hypovolaemic perturbations do not change AP, but reduce central venous, right heart and pulmonary pressures, and cause vasoconstriction. These observations have been interpreted as reflexes triggered by cardiopulmonary baroreceptors (Johnson *et al.* 1974; Pawelczyk & Raven, 1989). However, Taylor *et al.* (1995) showed that small reductions of effective blood volume reduce aortic baroreceptive areas and trigger haemodynamic adjustments which are so efficient that alterations in AP escape detection by conventional means. Accordingly, further studies are needed to understand the relative importance and mutual cooperation of arterial and cardiopulmonary baroreflexes in AP control during orthostatic stress.

Lastly, we used rabbits, which are quadrupeds. Since humans spend most of their time in nearly 90 deg upright postures whereas rabbits do not, our findings have limited applicability to humans. However, Japanese White rabbits spend most of their time in 10–40 deg head-up posture, and frequently stand up to nearly 70 deg. This suggests that rabbits have an ability to maintain arterial pressure against gravity-induced pressure perturbation under orthostatic stress. Additionally, in our preliminary experiments in rabbits, we observed that denervation of both carotid and aortic arterial baroreflexes caused postural hypotension of approximately 50 mmHg during 60 deg upright tilt, consistent with a previous study in rats (Sato *et al.* 2002). This suggests that even in quadrupeds, the arterial baroreflex has a very important role in the maintenance of AP under orthostatic stress. Accordingly, we speculate that our findings may reflect, at least, the qualitative aspects of orthostatic baroreflex physiology in humans. Indeed, recent human studies have suggested that orthostatic stress (lower body negative pressure) enhances the SNA response to arterial pressure change in the baroreflex closed-loop condition (Ichinose *et al.* 2004*a*; Ichinose *et al.* 2004*b*)

In conclusion, baroreflex open-loop equilibrium analysis demonstrated that 60 deg upright tilt shifted the baroreflex neural arc to a higher SNA and shifted the peripheral arc to a lower AP. Consequently, the upright tilt markedly increased the operating SNA and maintained the operating AP. Simulation study suggests that resetting of the neural arc would double the orthostatic activation of SNA and increase the operating AP in upright tilt by 10 mmHg compared with the absence of resetting. These data suggest that orthostatic stress increases SNA by resetting the baroreflex neural arc. The resetting of the neural arc may compensate for the reduced pressor responses to SNA in the peripheral cardiovascular system, and contribute to preventing postural hypotension.

References

Angell James JE (1971). The effects of changes of extramural, 'intrathoracic', pressure on aortic arch baroreceptors. *J Physiol* **214**, 89–103.

Cooke WH, Hoag JB, Crossman AA, Kuusela TA, Tahvanainen KU & Eckberg DL (1999). Human responses to upright tilt: a window on central autonomic integration. *J Physiol* **517**, 617–628.

Cooper VL & Hainsworth R (2001). Carotid baroreceptor reflexes in humans during orthostatic stress. *Exp Physiol* **86**, 677–681.

DiCarlo SE & Bishop VS (2001). Central baroreflex resetting as a means of increasing and decreasing sympathetic outflow and arterial pressure. *Ann N Y Acad Sci* **940**, 324–337.

Eckberg DL & Sleight P (1992). *Human Baroreflexes in Health and Disease*. Oxford University Press, New York.

Glantz SA (1997). *Primer of Biostatistics*, 4th edn. McGraw-Hill, New York.

Gotoh TM, Fujiki N, Matsuda T, Gao S & Morita H (2004). Roles of baroreflex and vestibulosympathetic reflex in controlling arterial blood pressure during gravitational stress in conscious rats. *Am J Physiol Regul Integr Comp Physiol* **286**, R25–R30.

Ichinose M, Saito M, Kitano A, Hayashi K, Kondo N & Nishiyasu T (2004*a*). Modulation of arterial baroreflex dynamic response during mild orthostatic stress in humans. *J Physiol* **557**, 321–330.

Ichinose M, Saito M, Ogawa T, Hayashi K, Kondo N & Nishiyasu T (2004*b*). Modulation of control of muscle sympathetic nerve activity during orthostatic stress in humans. *Am J Physiol Heart Circ Physiol* **287**, H2147–H2153.

Johnson JM, Rowell LB, Niederberger M & Eisman MM (1974). Human splanchnic and forearm vasoconstrictor responses to reductions of right atrial and aortic pressures. *Circ Res* **34**, 515–524.

Kaufmann H, Biaggioni I, Voustianiouk A, Diedrich A, Costa F, Clarke R, Gizzi M, Raphan T & Cohen B (2002). Vestibular control of sympathetic activity. An otolith-sympathetic reflex in humans. *Exp Brain Res* **143**, 463–469.

Kawada T, Shishido T, Inagaki M, Tatewaki T, Zheng C, Yanagiya Y, Sugimachi M & Sunagawa K (2001). Differential dynamic baroreflex regulation of cardiac and renal sympathetic nerve activities. *Am J Physiol Heart Circ Physiol* **280**, H1581–H1590.

Kawada T, Yanagiya Y, Uemura K, Miyamoto T, Zheng C, Li M, Sugimachi M & Sunagawa K (2003). Input-size dependence of the baroreflex neural arc transfer characteristics. *Am J Physiol Heart Circ Physiol* **284**, H404–H415.

Kent B, Drane J, Blumenstein B & Manning J (1972). A mathematical model to assess changes in the baroreceptor reflex. *Cardiology* **57**, 295–310.

Miki K, Yoshimoto M & Tanimizu M (2003). Acute shifts of baroreflex control of renal sympathetic nerve activity induced by treadmill exercise in rats. *J Physiol* **548**, 313–322.

Monahan KD & Ray CA (2002). Vestibulosympathetic reflex during orthostatic challenge in aging humans. *Am J Physiol Regul Integr Comp Physiol* **283**, R1027–R1032.

Morillo CA, Eckberg DL, Ellenbogen KA, Beightol LA, Hoag JB, Tahvanainen KU, Kuusela TA & Diedrich AM (1997). Vagal and sympathetic mechanisms in patients with orthostatic vasovagal syncope. *Circulation* **96**, 2509–2513.

Mosqueda-Garcia R, Furlan R, Fernandez-Violante R, Desai T, Snell M, Jarai Z, Ananthram V, Robertson RM & Robertson D (1997). Sympathetic and baroreceptor reflex function in neurally mediated syncope evoked by tilt. *J Clin Invest* **99**, 2736–2744.

Pawelczyk JA & Raven PB (1989). Reductions in central venous pressure improve carotid baroreflex responses in conscious men. *Am J Physiol* **257**, H1389–H1395.

Persson P, Ehmke H, Kirchheim H & Seller H (1988). Effect of sino-aortic denervation in comparison to cardiopulmonary deafferentiation on long-term blood pressure in conscious dogs. *Pflugers Arch* **411**, 160–166.

Persson P & Kirchheim H (1991). *Baroreceptor Reflexes: Integrative Functions and Clinical Aspects*. Springer-Verlag, Berlin.

Potts JT & Mitchell JH (1998). Rapid resetting of carotid baroreceptor reflex by afferent input from skeletal muscle receptors. *Am J Physiol* **275**, H2000–H2008.

Ray CA & Carter JR (2003). Vestibular activation of sympathetic nerve activity. *Acta Physiol Scand* **177**, 313–319.

Rea RF & Eckberg DL (1987). Carotid baroreceptor-muscle sympathetic relation in humans. *Am J Physiol* **253**, R929–R934.

Rowell LB (1993). *Human Cardiovascular Control*. Oxford University Press, New York.

Rudas L, Crossman AA, Morillo CA, Halliwill JR, Tahvanainen KU, Kuusela TA & Eckberg DL (1999). Human sympathetic and vagal baroreflex responses to sequential nitroprusside and phenylephrine. *Am J Physiol* **276**, H1691–H1698.

Sagawa K, Maughan L, Suga H & Sunagawa K (1988). *Cardiac Contraction and the Pressure-Volume Relationship*. Oxford University Press, New York.

Sato T, Kawada T, Inagaki M, Shishido T, Takaki H, Sugimachi M & Sunagawa K (1999). New analytic framework for understanding sympathetic baroreflex control of arterial pressure. *Am J Physiol* **276**, H2251–H2261.

Sato T, Kawada T, Sugimachi M & Sunagawa K (2002). Bionic technology revitalizes native baroreflex function in rats with baroreflex failure. *Circulation* **106**, 730–734.

Taylor JA, Halliwill JR, Brown TE, Hayano J & Eckberg DL (1995). 'Non-hypotensive' hypovalaemia reduces ascending aortic dimensions in humans. *J Physiol* **483**, 289–298.

Yamamoto K, Kawada T, Kamiya A, Takaki H, Miyamoto T, Sugimachi M & Sunagawa K (2004). Muscle mechanoreflex induces the pressor response by resetting the arterial baroreflex neural arc. *Am J Physiol* **286**, H1382–H1388.

Yates B (1992). Vestibular influence on the sympathetic nervous system. *Brain Res Brain Res Rev* **17**, 51–59.

Acknowledgements

This study was supported by Industrial Technology Research Grant Program, 03A47075, from New Energy and Industrial Technology Development Organization (NEDO) of Japan, by the Program for Promotion of Fundamental Studies in Health Science of the Organization for Pharmaceutical Safety and Research of Japan, and also by the Ground-based Research Announcement for Space Utilization promoted by Japan Space Forum.

Microdialysis separately monitors myocardial interstitial myoglobin during ischemia and reperfusion

Hirotoshi Kitagawa, Toji Yamazaki, Tsuyoshi Akiyama, Masaru Sugimachi, Kenji Sunagawa and Hidezo Mori

AJP - Heart 289:924-930, 2005. First published Apr 15, 2005; doi:10.1152/ajpheart.01207.2004

Am J Physiol Heart Circ Physiol 289: H924–H930, 2005.
First published April 15, 2005; doi:10.1152/ajpheart.01207.2004.

Microdialysis separately monitors myocardial interstitial myoglobin during ischemia and reperfusion

Hirotoshi Kitagawa,[1] Toji Yamazaki,[2] Tsuyoshi Akiyama,[2] Masaru Sugimachi,[3] Kenji Sunagawa,[4] and Hidezo Mori[2]

[1]*Department of Anesthesiology, Shiga University of Medical Science, Otsu; Departments of* [2]*Cardiac Physiology and* [3]*Cardiovascular Dynamics, National Cardiovascular Center Research Institute, Suita; and* [4]*Department of Cardiovascular Medicine, Kyushu University Graduate School of Medical Sciences, Fukuoka, Japan*

Submitted 1 December 2004; accepted in final form 6 April 2005

Kitagawa, Hirotoshi, Toji Yamazaki, Tsuyoshi Akiyama, Masaru Sugimachi, Kenji Sunagawa, and Hidezo Mori. Microdialysis separately monitors myocardial interstitial myoglobin during ischemia and reperfusion. *Am J Physiol Heart Circ Physiol* 289: H924–H930, 2005. First published April 15, 2005; doi:10.1152/ajpheart.01207.2004.—Direct monitoring of myoglobin efflux during ischemia and reperfusion has been limited because of inherent sample collection problems in the ischemic region. Recently, the cardiac dialysis technique has offered a powerful method for monitoring myocardial interstitial levels of low-molecular-weight compounds in the cardiac ischemic region. In the present study, we extended the molecular target to high-molecular-weight compounds by use of microdialysis probes with a high-molecular-mass cutoff and monitored myocardial interstitial myoglobin levels. A dialysis probe was implanted in the left ventricular free wall in anesthetized rabbits. The main coronary artery was occluded for 60 or 120 min. We examined the effects of myocardial ischemia and reperfusion on myocardial interstitial myoglobin levels. Interstitial myoglobin increased within 15 min of ischemia and continued to increase during 120 min of ischemia, whereas blood myoglobin increased at 45 min of ischemia. Lactate and myoglobin in the interstitial space increased during the same period. At 60 min of ischemia, reperfusion markedly accelerated interstitial myoglobin release. The interstitial myoglobin level was fivefold higher at 0–15 min of reperfusion than at 60–75 min of coronary occlusion. The dialysis technique permits earlier detection of myoglobin release and separately monitors myoglobin release during ischemia and reperfusion. Myocardial interstitial myoglobin levels can serve as an index of myocardial injury evoked by ischemia or reperfusion.

infarction; interstitial space; membrane permeability

IT IS WELL KNOWN that certain proteins, including myoglobin, called serum cardiac markers, are released into the bloodstream in large quantities from necrotic cardiac muscle cells after myocardial infarction (20, 26, 43). However, because direct samples from the ischemic region are not readily obtainable, in situ studies on efflux of these proteins in the cardiac ischemic region have been limited (22). This problem of sample collection from the ischemic region remains unresolved. First, it is uncertain exactly when cardiac markers appear from injured myocardium. The appearance of cardiac markers indicates the turning point from reversible injury to irreversible damage (43). However, the first appearance of cardiac markers in the bloodstream is influenced by the slow transport of cardiac markers from the interstitial space into the bloodstream (20). Thus the detection of this appearance is of great value in understanding the pathophysiological events induced by myocardial ischemia. Second, recent experimental and clinical findings suggest that reperfusion itself seems to accelerate the release of cardiac markers (18, 37, 38). However, the extent to which reperfusion contributes to relative changes in their release is unclear. To determine myocardial injury evoked by reperfusion, more information is needed about the extent to which ischemia and reperfusion affect changes in the release of cardiac markers. Third, present methods used to measure infarct size require tissue analysis several hours after the ischemic event (8). Furthermore, histochemical analysis depends on the times of ischemia and reperfusion (23, 33). Concise, dissociated assessments of ischemia and reperfusion injury have been a frequent object of research.

In general, mobilization of cardiac markers from ischemic myocardium to the bloodstream has been divided into two different sequences: release from the myocardial cell to the interstitial space and transport from the interstitial space into the bloodstream (20). Therefore, if we examine the first process in in situ myocardium, we can discuss the pathophysiological changes during development of ischemic myocardial necrosis. However, little information is available on interstitial protein kinetics in the ischemic region (15). Examination of protein kinetics in the ischemic region has been limited to assessment of protein kinetics in the isolated Langendorff-perfused heart (28, 39). Recently, a cardiac dialysis technique has provided a powerful method for monitoring myocardial interstitial levels of low-molecular-weight compounds in the cardiac ischemic region (2, 6, 14, 31). Furthermore, this method is suitable for distinguishing between ischemia and reperfusion responses (32). By improving the microdialysis probes with a high-molecular-mass cutoff membrane, we have extended the molecular target to high-molecular-weight peptides and proteins and monitored myocardial interstitial protein levels.

In the present study, we chose myoglobin as one of the earliest biochemical markers in myocardial injury (4, 34). We applied the dialysis technique to the heart of anesthetized rabbits and investigated myocardial interstitial myoglobin levels during coronary occlusion and reperfusion. To address the above-mentioned issues, we compared the first appearance of myocardial interstitial myoglobin levels with that of low-molecular-weight metabolites (lactate and glycerol). Further-

Address for reprint requests and other correspondence: T. Yamazaki, Dept. of Cardiac Physiology, National Cardiovascular Center Research Institute, 5-7-1 Fujishirodai, Suita, Osaka 565-8565, Japan (E-mail: yamazaki@ri.ncvc.go.jp).

The costs of publication of this article were defrayed in part by the payment of page charges. The article must therefore be hereby marked "*advertisement*" in accordance with 18 U.S.C. Section 1734 solely to indicate this fact.

more, we compared the time course of myocardial interstitial myoglobin during reperfusion after ischemia with that of sustained ischemia and examined the changes in myoglobin release evoked by reperfusion. The results of the present study indicate that microdialysis is suitable for distinguishing between ischemia and reperfusion injury.

MATERIALS AND METHODS

Animal Preparation

The investigation conformed with the *Guide for the Care and Use of Laboratory Animals* published by the National Institutes of Health (NIH Publication No. 85-23, Revised 1996). All protocols were approved by the Animal Subjects Committee of the National Cardiovascular Center. Thirty adult male Japanese White rabbits (2.5–3.2 kg) were anesthetized with pentobarbital sodium (30–35 mg/kg iv). The level of anesthesia was maintained with a continuous intravenous infusion of pentobarbital sodium (1–2 $mg \cdot kg^{-1} \cdot h^{-1}$). The rabbits were intubated and ventilated with room air mixed with oxygen. Body temperature was maintained at ~39°C with a heating pad and lamp. Heart rate (HR), mean arterial pressure (MAP), and electrocardiogram were monitored and recorded continuously. Heparin sodium (200 IU/kg) was first administered intravenously and then maintained with a continuous infusion (5–10 $IU \cdot kg^{-1} \cdot h^{-1}$) to prevent blood coagulation. With the animal in the lateral position, the fifth or sixth rib on the left side was partially removed to expose the heart. A small incision was made in the pericardium, and the dialysis probe was implanted in the region perfused by the left circumflex coronary artery (LCX) of the left ventricular wall. A snare was placed around the main branch of the LCX to act as the occluder for later coronary occlusion. To ensure that the sampling area was in the ischemic region, we examined the color and motion of the ventricular wall during a brief occlusion and confirmed that the dialysis probe was correctly located. To avoid a preconditioning effect, the duration of occlusion was limited to a few seconds.

Dialysis Technique

We designed a handmade long transverse dialysis probe (1). One end of a polyethylene tube (25 cm long, 0.5 mm OD, 0.2 mm ID) was dilated with a 27-gauge needle (0.4 mm OD). Each end of the dialysis fiber (8 mm long, 0.215 mm OD, 0.175 mm ID, 300 Å pore size; Evaflux type 5A, Kuraray Medical) was inserted into the polyethylene tube and glued. A fine guiding needle (25 mm long, 0.51 mm OD, 0.25 mm ID) was used for implantation of the dialysis probes. A guiding needle was connected to the dialysis probe with a stainless steel rod (5 mm long, 0.25 mm OD). At a perfusion speed of 5 μl/min, the in vitro recovery rate (RR) of myoglobin was 15 ± 0.6% (number of dialysis probes = 3). In vitro RR was defined as follows: $RR = (C_{in} - C_{out})/C_{in}$, where C_{in} and C_{out} are the concentrations of myoglobin in the perfusate and in the dialysate, respectively (19). For monitoring myocardial interstitial lactate and glycerol levels, we used a conventional dialysis fiber (PAN-1200, Asahi Chemical Japan) to detect low-molecular-weight compounds (1).

Dialysis probes were perfused with Ringer solution (in mM: 147.0 NaCl, 4.0 KCl, and 2.25 $CaCl_2$) at 5 μl/min using a microinjection pump (model CMA/100, Carnegie Medicine). Figure 1 shows the time course of dialysate myoglobin levels collected at 1-h intervals over a 4-h period after probe implantation. Dialysate myoglobin rapidly decreased to 261 ± 56 ng/ml at 2 h after probe implantation. Thereafter, it gradually decreased, reaching an almost steady level of 222 ± 37 ng/ml 4 h after probe implantation. On the basis of the results of this experiment, in the subsequent protocol, we discarded the first 120-min collections of dialysate and measured the dialysate myoglobin level twice at 30-min intervals. When dialysate myoglobin levels reached the steady level, we started the experimental protocol.

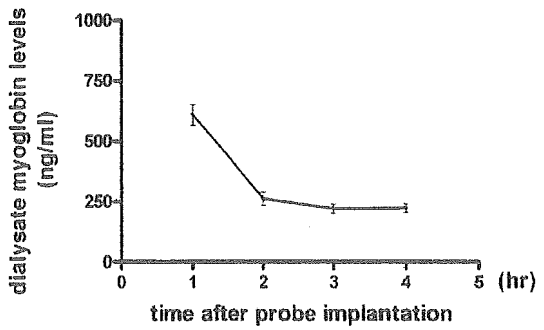

Fig. 1. Time course of dialysate myoglobin levels after probe implantation. Dialysate myoglobin levels decreased over the first 2 h and then reached an almost steady level. Values are means ± SE from 5 rabbits.

Sampling periods were 15 min (1 sampling volume = 75 μl) in control and during occlusion and reperfusion. Taking into consideration the dead space between the dialysis fiber and sample tube, we sampled the dialysate.

Dialysate myoglobin concentrations were measured as an index of myocardial interstitial myoglobin levels. Blood samples were obtained from the femoral artery. Using immunochemistry (Cardiac Reader, Roche Diagnostics), we measured the myoglobin levels (7). The detection limit of myoglobin was 30 ng/ml. The dialysate lactate and glycerol levels were measured by kinetic enzymatic analysis (CMA 600 analyzer, Carnegie Medicine) (30).

Experimental Protocols

After control sampling, we occluded the main branch of the LCX for 60 min and then released the occluder. We continuously sampled the dialysate from the ischemic region during 60 min of coronary occlusion and reperfusion.

Time course of dialysate lactate, glycerol, and myoglobin levels during myocardial ischemia. We compared the dialysate myoglobin levels with the blood myoglobin levels. After control sampling, we observed the time course of dialysate and blood myoglobin levels during 60 min of coronary occlusion. In addition, we measured simultaneously dialysate lactate and glycerol levels from the ischemic region in separate rabbits.

Time course of dialysate myoglobin levels during 60 min of reperfusion following 60 and 120 min of ischemia. Reperfusion modulates myocardial membrane damage and may accelerate dialysate myoglobin levels (18, 21, 37). We compared the time course of dialysate myoglobin during 60 min of reperfusion following 60 min of ischemia with that of 120 min of ischemia.

Time course of dialysate myoglobin levels during local administration of cyanide. To confirm whether the dialysate myoglobin level reflects myocardial damage evoked by ischemia or hypoxia, we tested the effect of local sodium cyanide (NaCN) administration on dialysate myoglobin levels. We collected a control dialysis sample and then replaced the perfusate with Ringer solution containing NaCN (30 mM), thereby locally administering NaCN for 60 min. We obtained four consecutive dialysate samples and measured the dialysate myoglobin levels.

At the end of each experiment, the rabbits were killed with an overdose of pentobarbital sodium, and the implant regions were checked to confirm that the dialysis probes had been implanted within the cardiac muscle.

Statistical Analysis

Dialysate lactate, glycerol, and myoglobin responses to coronary occlusion were statistically analyzed by one-way analysis of variance with repeated measures. When a statistically significant effect of

Table 1. *Changes in HR and MAP in coronary artery occlusion*

	120 min Coronary Occlusion								
	C	5	15	30	45	60	75	90	105
HR, beats/min	268±7	264±8	242±8*	250±3*	253±4*	252±4*	250±4*	251±3*	248±4*
MAP, mmHg	84±4	74±5*	69±5*	71±5*	68±5*	67±5*	66±4*	65±4*	64±5*
	60 min Occlusion - 60 min Reperfusion								
	C	5	15	30	45	R5	R15	R30	R45
HR, beats/min	274±9	261±6*	255±7*	254±6*	261±7*	256±5*	263±10*	264±12*	263±9*
MAP, mmHg	78±4	67±3*	65±2*	67±2*	65±2*	61±2*	60±3*†	61±2*	58±2*†

Values are mean ± SE. Data were obtained during control (C), after 5, 15, 30, 45, 60, 75, 90, and 105 min of coronary artery occlusion, and after 5, 15, 30, and 45 min of reperfusion (R). *$P < 0.05$ vs. control. †$P < 0.05$ vs. 45 min occlusion.

coronary occlusion was detected as a whole, the Newman-Keuls test was applied to determine which mean values differed significantly from each other (40). Statistical significance was defined as $P < 0.05$. Values are means ± SE.

RESULTS

Time Course of HR and MAP

Table 1 shows the time courses of HR and MAP during coronary occlusion and reperfusion. Coronary occlusion decreased HR and MAP. Reperfusion did not alter HR but temporarily decreased MAP.

Time Course of Dialysate Lactate, Glycerol, and Myoglobin Levels During Myocardial Ischemia

Coronary occlusion significantly altered dialysate myoglobin levels (Fig. 2). Dialysate myoglobin levels increased significantly from 168 ± 32 ng/ml in the control to 570 ± 107 ng/ml at 0–15 min of occlusion. During 60 min of coronary occlusion, dialysate myoglobin levels progressively increased and reached 2,583 ± 208 ng/ml at 45–60 min of occlusion. A significant increase in blood myoglobin occurred at 45–60 min of coronary occlusion. Dialysate lactate levels were 1.00 ± 0.21 mmol/l in the control and increased after coronary occlusion (Fig. 3). During 60 min of coronary occlusion, dialysate lactate levels markedly increased and reached 3.34 ± 0.50 mmol/l at 45–60 min of occlusion. During 60 min of coronary occlusion, dialysate glycerol levels also increased and reached 232 ± 33 μmol/l at 45–60 min of occlusion.

Time Course of Dialysate Myoglobin Levels During 60 min of Reperfusion Following 60 and 120 Minutes of Ischemia

There were no significant differences in the control dialysate myoglobin levels between the two groups (Fig. 4). During ischemia, the dialysate myoglobin levels progressively increased and reached 4,054 ± 659 ng/ml at 105–120 min of coronary occlusion. During 60 min of coronary occlusion, there were no statistically significant differences in the dialysate myoglobin levels between the two groups. After release of the occluder, the dialysate myoglobin levels markedly increased to 12,569 ± 2,347 ng/ml at 0–15 min of reperfusion. The dialysate myoglobin levels at 0–15 min of reperfusion were fivefold higher than those at 60–75 min of 120 min of coronary occlusion. Furthermore, these values were higher than peak levels during 120 min of coronary occlusion. The

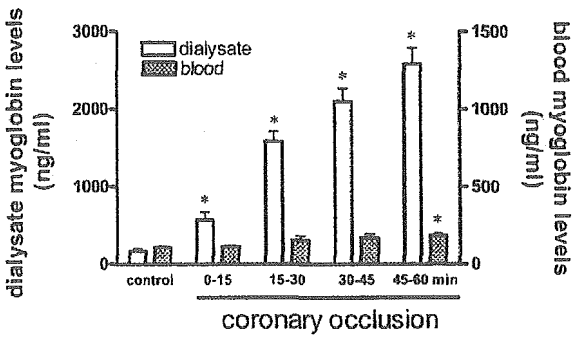

Fig. 2. Time courses of dialysate and blood myoglobin levels during 60 min of ischemia. Values are means ± SE. *$P < 0.05$ vs. control.

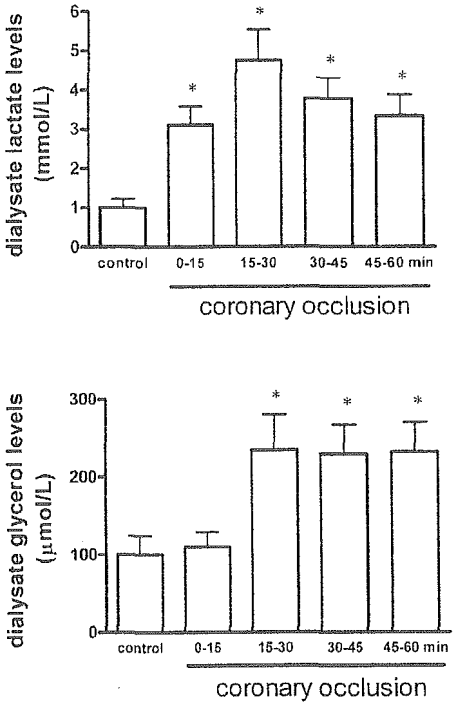

Fig. 3. Time courses of dialysate lactate (*top*) and glycerol (*bottom*) levels during 60 min of ischemia. Values are means ± SE. *$P < 0.05$ vs. control.

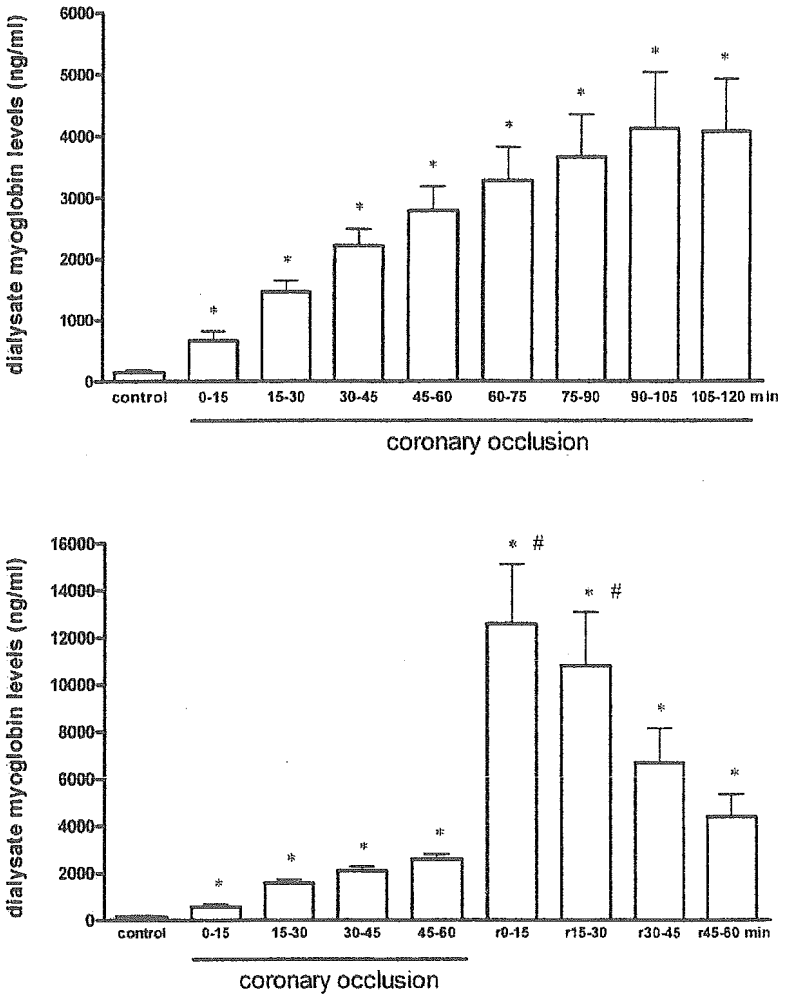

Fig. 4. Time courses of dialysate myoglobin levels during 120 min of ischemia (*top*) and 60 min of ischemia followed by 60 min of reperfusion (r, *bottom*). Values are means ± SE. $^{*}P < 0.05$ vs. control. $^{\#}P < 0.05$ vs. 45–60 min of occlusion.

dialysate myoglobin levels gradually decreased and reached 4,391 ± 879 ng/ml at 45–60 of reperfusion. At 0–15 min of reperfusion, dialysate lactate and glycerol levels were 3.27 ± 0.61 mmol/l and 242 ± 37.7 μmol/l, respectively. Dialysate lactate and glycerol levels remained unchanged at 0–15 min of reperfusion.

Time Course of Dialysate Myoglobin Levels During Local Administration of NaCN

Local administration of NaCN increased the dialysate myoglobin levels (Fig. 5). This increase was statistically significant compared with the control level at all collection periods during NaCN administration, except at 0–15 min. The maximum myoglobin level was comparable to that observed during 60 min of ischemia.

DISCUSSION

Using the dialysis technique in the in vivo rabbit heart, we observed myocardial interstitial myoglobin levels during myocardial ischemia and reperfusion. Our data demonstrated myoglobin release in the early stage of cardiac ischemia and its enhancement by reperfusion. We discuss here the time course of myocardial myoglobin release during coronary occlusion and after reperfusion.

We show for the first time that myoglobin release increases within 15 min of ischemia and continues to increase during 60 min of ischemia. However, significant changes in the blood myoglobin level occurred at 45–60 min of coronary occlusion. Our data suggest a contrast between blood and dialysate

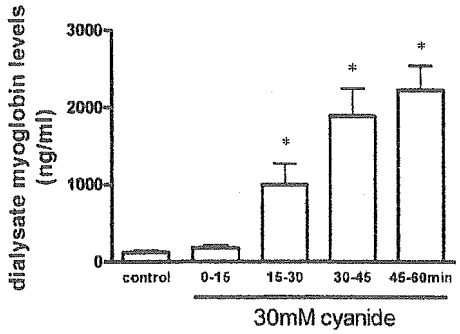

Fig. 5. Time course of dialysate myoglobin levels during local administration of sodium cyanide (30 mM). Values are means ± SE. $^{*}P < 0.05$ vs. control.

myoglobin levels during ischemia. The delay of the first appearance of myoglobin in the bloodstream is mainly due to the slow transport of myoglobin from the interstitial space into the bloodstream (20). Therefore, myoglobin concentration measured by cardiac microdialysis provides information regarding early release of cytosol protein into the interstitial space. Within the 15-min time resolution, this increase in myoglobin release was accompanied by increases in interstitial lactate. Dead space volume between the dialysis fiber and the sample microtube was identical for lactate, glycerol, and myoglobin. The currently accepted concept (20) is that leakage of anaerobic metabolites precedes macromolecular protein release during ischemia. Anaerobic metabolites accumulate and leak from the ischemic region within minutes via diffusion or transport (6, 12, 41). In contrast to low-molecular-weight metabolites, macromolecular proteins could be released into the interstitial space without cytosol accumulation of myoglobin, probably via bleb or altered permeability. Although sampling periods of 15 min are too long to enable us to distinguish the rate of release of lactate vs. myoglobin, our data at least suggest that cellular metabolic derangement is involved in membrane disruption for myoglobin release.

Myocardial injury caused by ischemia-reperfusion is associated with membrane phospholipid degradation, which is thought to underlie disruption of the cell membrane (27). Glycerol is an end product of membrane phospholipid degradation and has been used to study membrane phospholipid degradation after cerebral ischemia and seizures (12). In the present study, dialysate glycerol was examined as a potential marker for membrane phospholipid degradation in myocardial ischemia and reperfusion. We observed increases in dialysate glycerol levels during 15–60 min of ischemia but not during reperfusion. In general, phospholipid degradation is accentuated during reperfusion (27). Therefore, dialysate glycerol is not suitable as an index of membrane phospholipid degradation, and the release of glycerol from membrane phospholipid degradation might be too small to allow detection in blood-perfused heart.

Early change of cytosol myoglobin was detected by immunofluorescence after occlusion of the coronary artery (16, 25). Histochemical studies demonstrated that intracellular diffusion of cytosol myoglobin into the nuclei and mitochondria was evident as early as 0.5 h after coronary artery occlusion (17, 25). Our data demonstrate early loss of cytosol myoglobin into the interstitial space. Release of cytosol protein is caused by membrane damage via alteration of permeability or bleb formation. Blebs appeared on the cell surfaces, and the cell began to swell within 10–20 min of ATP depletion in a glia cell line or hepatocytes (13, 24). Furthermore, NMR spectroscopy suggested that sarcolemmal membranes are gradually permeabilized to large molecules by ischemia (3). These alterations of sarcolemmal membranes might be involved in early release of myoglobin during the myocardial ischemia. Our method offers extremely fast and sensitive analysis of membrane injury in myocardial ischemia that is not evident by histological or blood analysis. Quantitative assessment of interstitial myoglobin levels could be performed independently of reperfusion cell injury and could be helpful in devising various myocardial preservation treatments.

We show that reperfusion markedly accelerates myoglobin release in the ischemic region. The interstitial myoglobin levels at 0–15 min of reperfusion were fivefold higher than those at 60–75 min of 120 min of coronary occlusion. During the reperfusion period, interstitial accumulated myoglobin might be washed out into the bloodstream (37). Therefore, the amount of released myoglobin at reperfusion could be markedly greater than the changes in interstitial myoglobin concentrations at reperfusion. Release of cytosolic protein resulted from a disruption of a sarcolemmal bleb or an enhancement of membrane permeability (5, 29, 35). Either condition may gain relevance during the reperfusion period. Thus the release of myoglobin during the reperfusion seems to serve as an index of disrupted sarcolemmal membrane.

Although the exact mechanisms of accelerated myoglobin release cannot be determined from the present study, our data suggest that substances induced during reperfusion differ from those induced during ischemia. Reperfusion enhanced myoglobin release but did not accelerate lactate or glycerol release in the interstitial space, whereas ischemia accompanied macromolecular myoglobin release as well as anaerobic metabolite release. Furthermore, in the previous studies, neither catecholamine nor acetylcholine release was accelerated by reperfusion in ischemic cardiac sympathetic and parasympathetic nerve endings (2, 14). During reperfusion, surviving myocardial cells and nerve terminals quickly recover aerobic metabolism and take up these accumulated substances, whereas myocardial cells have no capability of myoglobin uptake via the sarcolemmal membrane, leading to continued myoglobin release via the disrupted membrane. Reperfusion may enhance membrane permeability (5). Further disruption of membrane blebs may cause rupture of the membrane (29, 35). Alternatively, in isolated perfused rats, leakage of cytoplasmic enzymes during reoxygenation is accelerated by cardiac revived beating, because the cell membrane becomes fragile during the preceding anoxia (36). In either condition, reperfusion-induced breakdown of membrane phospholipids contributes to an alteration of permeability or bleb formation (27). Disruption of the membrane phospholipid bilayer is likely to play a role in myoglobin release from the cytosome into the interstitial spaces.

In the present study, we demonstrate that loss of cytosol myoglobin occurs during myocardial ischemia and reperfusion and might be involved in the outcome and pathophysiology of the ischemic heart. Loss of cytosol myoglobin may precede, at least in part, histological evidence of necrosis and occur in the remaining viable myocardium that is not necrotic (11). In vertebrate heart, myoglobin is involved in the transport of oxygen from the sarcolemma to the mitochondria (42). Recent studies from myoglobin knockout mice indicate that myoglobin contributes to the scavenging of bioactive nitric oxide (NO) or oxygen radicals during ischemia-reperfusion (9, 10). NO production and/or oxidant injury occur during the reperfusion period. In hearts lacking myoglobin, changes in NO and oxidative stress have a much larger impact on the maintenance of vascular tone and cardiac function (44). Similarly, in myoglobin knockout mice, loss of cytosol myoglobin may be involved in the delayed restoration of cardiac contractility in the postischemic region.

There are several limitations to the present study. First, with application of the dialysis technique to the heart, we had to perform this experiment as an acute surgical preparation. Probe implantation and/or surgical preparation might affect the con-

centration of myocardial interstitial myoglobin. To examine the effect of probe implantation and/or surgery, we performed the preliminary experiment on brief occlusion (3 min). Three minutes of coronary occlusion did not alter dialysate myoglobin levels. Furthermore, to confirm whether the dialysate myoglobin level reflects myocardial damage evoked by ischemia or hypoxia, we tested the effect of local NaCN administration on dialysate myoglobin levels: with NaCN, we found increases in dialysate myoglobin levels similar to the increase evoked by myocardial ischemia. Therefore, we believe that dialysate myoglobin levels reflect the release of myoglobin evoked by ischemia as well as by chemical hypoxia. The absolute myoglobin level might be affected by implantation and/or surgical preparation. However, it is possible to estimate myoglobin release from relative changes in myoglobin levels.

Second, in the present study, myocardial interstitial myoglobin levels during coronary occlusion and reperfusion were determined regionally. We implanted the dialysis probe in the midwall of the left ventricle. When the dialysis probe was implanted in the subendocardial zone, it is likely that subendocardial ischemia was much more severe than in the midwall, where the sampling was performed. Actually, subendocardial lactate was significantly greater than epicardial lactate during severe ischemia in the anesthetized dogs (6). Further studies are warranted concerning the influence of the ischemic area (subendocardial or marginal zone) on its myocardial interstitial myoglobin levels.

In summary, this microdialysis study in an ischemic animal model shows that coronary occlusion induced myoglobin release in minutes. Micromolecular metabolite (lactate) and macromolecular protein (myoglobin) increased during the first 15 min of ischemia. Reperfusion markedly enhanced myoglobin release without increases in lactate or glycerol levels. Elevation of myoglobin release represents an increase in sarcolemmal permeability or bleb formation during ischemia and reperfusion. Massive disruption of myocardial membrane occurs immediately after ischemia and is markedly accelerated by reperfusion. The dialysis technique permits more concise in vivo monitoring of myocardial membrane disruption during ischemia and reperfusion separately.

GRANTS

This study was supported by the Program for Promotion of Fundamental Studies in Health Science of the Organization for Pharmaceutical Safety and Research by grants-in-aid for scientific research from the Ministry of Education, Science.

REFERENCES

1. **Akiyama T, Yamazaki T, and Ninomiya I.** In vivo monitoring of myocardial interstitial norepinephrine by dialysis technique. *Am J Physiol Heart Circ Physiol* 261: H1643–H1647, 1991.
2. **Akiyama T, Yamazaki T, and Ninomiya I.** Differential regional response of myocardial interstitial noradrenaline levels to coronary occlusion. *Cardiovasc Res* 27: 817–822, 1993.
3. **Askenasy N, Vivi A, Tassini M, Navon G, and Farkas DL.** NMR spectroscopic characterization of sarcolemmal permeability during myocardial ischemia and reperfusion. *J Mol Cell Cardiol* 33: 1421–1433, 2001.
4. **Block MI, Said JW, Siegel RJ, and Fishbein MC.** Myocardial myoglobin following coronary artery occlusion. An immunohistochemical study. *Am J Pathol* 111: 374–379, 1983.
5. **Camilleri JP, Joseph D, Amat D, and Fabiani JN.** Impaired sacrolemmal membrane permeability in reperfused ischemic myocardium. Ultrastructual tracer study. *Virchows Arch* 388: 69–76, 1980.
6. **Delyani JA and Van Wylen GDL.** Endocardial and epicardial interstitial purines and lactate during graded ischemia. *Am J Physiol Heart Circ Physiol* 266: H1019–H1026, 1994.
7. **Dominici R, Infusino I, Valente C, Moraschineli I, and Franzini C.** Plasma or serum samples: measurements of cardiac troponin T and of other analytes compared. *Clin Chem Lab Med* 42: 945–951, 2004.
8. **Farb A, Kolodgie FD, Jones RM, Jenkins M, and Virmani R.** Early detection and measurement of experimental myocardial infarcts with horseradish peroxidase. *J Mol Cell Cardiol* 25: 343–353, 1993.
9. **Flögel U, Gödecke A, Klotz LO, and Schrader J.** Role of myoglobin in the antioxidant defense of the heart. *FASEB J* 18: 1156–1158, 2004.
10. **Flögel U, Merx MW, Gödecke A, Decking UKM, and Schrader J.** Myoglobin: a scavenger of bioactive NO. *Proc Natl Acad Sci USA* 98: 735–740, 2001.
11. **Heyndrickx GR, Amano J, Kenna T, Fallon JT, Patrick TA, Manders WT, Rogers GG, Rosendorff C, and Vatner SF.** Creatine kinase release not associated with myocardial necrosis after short periods of coronary artery occlusion in conscious baboons. *J Am Coll Cardiol* 6: 1299–1303, 1985.
12. **Hillered L, Valtysson J, Enblad P, and Persson L.** Interstitial glycerol as a marker for membrane phospholipid degradation in the acutely injured human brain. *J Neurol Neurosurg Psychiatry* 64: 486–491, 1998.
13. **Jurkowitz-Alexander MS, Altschuld RA, Hohl CM, Johnson JD, McDonald JS, Simmonds TD, and Horrocks LA.** Cell swelling, blebbing, and death are dependent on ATP depletion and independent of calcium during chemical hypoxia in a glial cell line (ROC-1). *J Neurochem* 59: 344–352, 1992.
14. **Kawada T, Yamazaki T, Akiyama T, Sato T, Shishido T, Inagaki M, Sugimachi M, and Sunagawa K.** Differential acetylcholine release mechanisms in the ischemic and non-ischemic myocardium. *J Mol Cell Cardiol* 32: 405–414, 2000.
15. **Kennergren C, Nyström B, Nyström U, Berglin E, Larsson G, Mantovani V, Lönnroth P, and Hamberger A.** In situ detection of myocardial infarction in pig by measurements of asparate aminotransferase (ASAT) activity in the interstitial fluid. *Scand Cardiovasc J* 31: 343–349, 1997.
16. **Kent SP.** Diffusion of myoglobin in the diagnosis of early myocardial ischemia. *Lab Invest* 46: 265–270, 1982.
17. **Kent SP.** Intracellular diffusion of myoglobin. A manifestation of early cell injury in myocardial ischemia in dogs. *Arch Pathol Lab Med* 108: 827–830, 1984.
18. **Laperche T, Steg PG, Dehoux M, Benessiano J, Grollier G, Aliot E, Mossard JM, Aubry P, Coisne D, Hanssen M, and Iliou MC.** A study of biochemical markers of reperfusion early after thrombolysis for acute myocardial infarction. The PERM Study Group Prospective Evaluation of Reperfusion Markers. *Circulation* 92: 2079–2088, 1995.
19. **Le Quellec A, Dupin S, Genissel P, Savin S, Marchand B, and Houin G.** Microdialysis probes calibration: gradient and tissue dependent changes in no net flux and reverse dialysis methods. *J Pharmacol Toxicol Methods* 33: 11–16, 1995.
20. **Mair J.** Tissue release of cardiac markers: from physiology to clinical applications. *Clin Chem Lab Med* 37: 1077–1084, 1999.
21. **Matsumura K, Jeremy RW, Schaper J, and Becker LC.** Progression of myocardial necrosis during reperfusion of ischemic myocardium. *Circulation* 97: 795–804, 1998.
22. **Miura T.** Does reperfusion induce myocardial necrosis? *Circulation* 82: 1070–1072, 1990.
23. **Nachlas MM and Shnitka TK.** Macroscopic identification of early myocardial infarcts by alterations in dehydrogenase activity. *Am J Pathol* 42: 379–405, 1963.
24. **Nieminen AL, Gores GJ, Wray BE, Tanaka Y, Herman B, and Lemasters JJ.** Calcium dependence of bleb formation and cell death in hepatocytes. *Cell Calcium* 9: 237–246, 1988.
25. **Nomoto K, Mori N, Miyamoto J, Shoji T, and Nakamura K.** Relationship between sarcolemmal damage and appearance of amorphous matrix densities in mitochondria following occlusion of coronary artery in rats. *Exp Mol Pathol* 51: 231–242, 1989.
26. **Ortmann C, Pfeiffer H, and Brinkmann B.** A comparative study on the immunohistochemical detection of early myocardial damage. *Int J Legal Med* 113: 215–220, 2000.
27. **Prasad MR, Popescu LM, Moraru II, Liu X, Maity S, Engelman RM, and Das DK.** Role of phospholipases A_2 and C in myocardial ischemic reperfusion injury. *Am J Physiol Heart Circ Physiol* 260: H877–H883, 1991.

28. **Remppis A, Scheffold T, Greten J, Haass M, Greten T, Kubler W, and Katus HA.** Intracellular compartmentation of troponin T: release kinetics after global ischemia and calcium paradox in the isolated perfused rat heart. *J Mol Cell Cardiol* 27: 793–803, 1995.
29. **Sage MD and Jennings RB.** Cytoskeletal injury and subsarcolemmal bleb formation in dog heart during in vitro total ischemia. *Am J Pathol* 133: 327–337, 1988.
30. **Sarrafzadeh AS, Sakowitz OW, Kiening KL, Benndorf G, Lanksch WR, and Unterberg AW.** Bedside microdialysis: a tool to monitor cerebral metabolism in subarachnoid hemorrhage patients? *Crit Care Med* 30: 1062–1070, 2002.
31. **Shindo T, Akiyama T, Yamazaki T, and Ninomiya I.** Increase in myocardial norepinephrine during a short period of coronary occlusion. *J Auton Nerv Syst* 48: 91–96, 1994.
32. **Shindo T, Akiyama T, Yamazaki T, and Ninomiya I.** Regional myocardial interstitial norepinephrine kinetics during coronary occlusion and reperfusion. *Am J Physiol Heart Circ Physiol* 270: H245–H251, 1996.
33. **Shirato C, Miura T, Ooiwa H, Toyofuku T, Wilborn WH, and Downey JM.** Tetrazolium artifactually indicates superoxide dismutase-induced salvage in reperfused rabbit heart. *J Mol Cell Cardiol* 21: 1187–1193, 1989.
34. **Spangenthal EJ and Ellis AK.** Cardiac and skeletal muscle myoglobin release after reperfusion of injured myocardium in dogs with systemic hypotension. *Circulation* 91: 2635–2641, 1995.
35. **Steenbergen C, Hill ML, and Jennings RB.** Volume regulation and plasma membrane injury in aerobic, anaerobic, and ischemic myocardium in vitro. Effects of osmotic cell swelling on plasma membrane integrity. *Circ Res* 57: 864–875, 1985.
36. **Takami H, Matsuda H, Kuki S, Nishimura M, Kawashima Y, Watari H, Furuya E, and Tagawa K.** Leakage of cytoplasmic enzymes from rat heart by the stress of cardiac beating after increase in cell membrane fragility by anoxia. *Pflügers Arch* 416: 144–150, 1990.
37. **Van der Laarse A, van der Wall EE, van den Pol RC, Vermeer F, Verheugt FW, Krauss XH, Bar FW, Hermens WT, Willems GW, and Simoons ML.** Rapid enzyme release from acutely infarcted myocardium after early thrombolytic therapy: washout or reperfusion damage? *Am Heart J* 115: 711–716, 1988.
38. **Van Kreel BK, van den Veen FH, Willems GM, and Hermens WT.** Circulatory models in assessment of cardiac enzyme release in dogs. *Am J Physiol Heart Circ Physiol* 264: H747–H757, 1993.
39. **Van Nieuwenhoven FA, Musters RJ, Post JA, Verkleij AJ, Van der Vusse GJ, and Glatz JF.** Release of proteins from isolated neonatal rat cardiomyocytes subjected to simulated ischemia or metabolic inhibition is independent of molecular mass. *J Mol Cell Cardiol* 28: 1429–1434, 1996.
40. **Wiener BJ.** *Statistical Principles in Experimental Design* (2nd ed.). New York: McGraw-Hill, 1971.
41. **Wikström G, Ronquist G, Nilsson S, Maripu E, and Waldenström A.** Continuous monitoring of energy metabolites using microdialysis during myocardial ischaemia in the pig. *Eur Heart J* 16: 339–347, 1995.
42. **Wittenberg JB and Wittenberg BA.** Myoglobin function reassessed. *J Exp Biol* 206: 2011–2020, 2003.
43. **Wu AH.** Biochemical markers of cardiac damage: from traditional enzymes to cardiac-specific proteins. IFCC Subcommittee on Standardization of Cardiac Markers (S-SCM). *Scand J Clin Lab Invest Suppl* 230: 74–82, 1999.
44. **Wunderlich C, Flögel U, Gödecke A, Heger J, and Schrader J.** Acute inhibition of myoglobin impairs contractility and energy state of iNOS-overexpressing hearts. *Circ Res* 92: 1352–1358, 2003.

Am J Physiol Heart Circ Physiol 289: H301–H307, 2005.
First published February 11, 2005; doi:10.1152/ajpheart.01237.2004.

Prediction of circulatory equilibrium in response to changes in stressed blood volume

Kazunori Uemura,[1] Toru Kawada,[1] Atsunori Kamiya,[1] Takeshi Aiba,[1,2] Ichiro Hidaka,[1,3] Kenji Sunagawa,[4] and Masaru Sugimachi[1]

[1]*Department of Cardiovascular Dynamics, National Cardiovascular Center Research Institute, Suita;* [2]*Pharmaceuticals and Medical Devices Agency, Tokyo;* [3]*Japan Association for the Advancement of Medical Equipment, Tokyo; and* [4]*Department of Cardiovascular Medicine, Kyushu University Graduate School of Medical Science, Fukuoka, Japan*

Submitted 7 December 2004; accepted in final form 4 February 2005

Uemura, Kazunori, Toru Kawada, Atsunori Kamiya, Takeshi Aiba, Ichiro Hidaka, Kenji Sunagawa, and Masaru Sugimachi. Prediction of circulatory equilibrium in response to changes in stressed blood volume. *Am J Physiol Heart Circ Physiol* 289: H301–H307, 2005. First published February 11, 2005; doi:10.1152/ajpheart.01237.2004.—Accurate prediction of cardiac output (CO), left atrial pressure (P_{LA}), and right atrial pressure (P_{RA}) is a prerequisite for management of patients with compromised hemodynamics. In our previous study (Uemura et al. *Am J Physiol Heart Circ Physiol* 286: H2376–H2385, 2004), we demonstrated a circulatory equilibrium framework, which permits the prediction of CO, P_{LA}, and P_{RA} once the venous return surface and integrated CO curve are known. Inasmuch as we also showed that the surface can be estimated from single-point CO, P_{LA}, and P_{RA} measurements, we hypothesized that a similar single-point estimation of the CO curve would enable us to predict hemodynamics. In seven dogs, we measured the P_{LA}-CO and P_{RA}-CO relations and derived a standardized CO curve using the logarithmic function $CO = S_L[\ln(P_{LA} - 2.03) + 0.80]$ for the left heart and $CO = S_R[\ln(P_{RA} - 2.13) + 1.90]$ for the right heart, where S_L and S_R represent the preload sensitivity of CO, i.e., pumping ability, of the left and right heart, respectively. To estimate the integrated CO curve in each animal, we calculated S_L and S_R from single-point CO, P_{LA}, and P_{RA} measurements. Estimated and measured CO agreed reasonably well. In another eight dogs, we altered stressed blood volume (−8 to +8 ml/kg of reference volume) under normal and heart failure conditions and predicted the hemodynamics by intersecting the surface and the CO curve thus estimated. We could predict CO [$y = 0.93x + 6.5$, $r^2 = 0.96$, standard error of estimate (SEE) = 7.5 ml·min^{-1}·kg^{-1}], P_{LA} ($y = 0.90x + 0.5$, $r^2 = 0.93$, SEE = 1.4 mmHg), and P_{RA} ($y = 0.87x + 0.4$, $r^2 = 0.91$, SEE = 0.4 mmHg) reasonably well. In conclusion, single-point estimation of the integrated CO curve enables accurate prediction of hemodynamics in response to extensive changes in stressed blood volume.

logarithmic function; venous return surface; heart failure

ACCURATE PREDICTION of cardiac output (CO) and cardiac filling pressures after therapeutic interventions is indispensable for optimal management and improved prognosis of patients with compromised hemodynamics (4, 5, 13, 23). In the 1980s, Sunagawa's group (20, 27) extended the framework of circulatory equilibrium of Guyton and co-workers (9, 10) to analyze complicated hemodynamic conditions such as left-sided heart failure. The extended framework is composed of a venous return surface representing the venous return of the systemic and pulmonary circulations and an integrated CO curve representing the pumping ability of the left and the right heart (Fig. 1) (27). The intersection point of the venous return surface and the integrated cardiac curve gives the equilibrium CO, left atrial pressure (P_{LA}), and right atrial pressure (P_{RA}). Changes in stressed blood volume shift the venous return surface upward or downward, altering the equilibrium point accordingly.

Our previous study (29) experimentally validated that venous return is a linear function of P_{LA} and P_{RA} and that this relation is expressed by a flat surface, i.e., the venous return surface (Fig. 1). In addition, because of the small intra- and interanimal variability in the slope of the surface, only a single set of CO, P_{LA}, and P_{RA} values is sufficient to estimate the venous return surface. Furthermore, it is possible to predict how the venous return surface shifts in response to a known amount of change in the stressed blood volume. These findings suggest that if the integrated CO curve can be estimated from a single set of CO, P_{LA}, and P_{RA} values, it is possible to predict hemodynamics in response to various therapeutic interventions, which induce changes in loading condition or in the pumping ability of the heart (29). The present study was therefore undertaken to develop a method to estimate the integrated CO curve from a single set of CO, P_{LA}, and P_{RA} values and to examine whether intersection of the integrated CO curve and the venous return surface thus estimated predicts hemodynamics in response to extensive changes in the stressed blood volume. Using our model, we were able to estimate the CO curve and predict the hemodynamics in anesthetized, open-chest dogs under conditions of left heart failure as well as normal cardiac function.

METHODS

Integrated CO Curve

In our previous study, we showed that CO is closely related to P_{LA} or P_{RA} by a three-parameter logarithmic function (29)

$$CO = S_L \times [\ln (P_{LA} - F_L) + H_L] \quad (1)$$

$$CO = S_R \times [\ln (P_{RA} - F_R) + H_R] \quad (2)$$

where S_L, F_L, and H_L and S_R, F_R, and H_R are parameters.

To estimate the integrated CO curve from a single set of CO, P_{LA}, and P_{RA} values, we fixed the F and H parameters according to the following rationale. It is well known that the CO curve varies widely with changes in ventricular contractility, heart rate, vascular resistance, and diastolic stiffness (8, 10, 20, 21, 24, 30). As shown in the APPENDIX, these factors are mainly included in the S parameter rather than in the F or H parameters. The S parameter thus comprehensively

Address for reprint requests and other correspondence: K. Uemura, Dept. of Cardiovascular Dynamics, National Cardiovascular Center Research Institute, 5-7-1 Fujishirodai, Suita 565-8565, Japan (E-mail: kuemura@ri.ncvc.go.jp).

The costs of publication of this article were defrayed in part by the payment of page charges. The article must therefore be hereby marked "*advertisement*" in accordance with 18 U.S.C. Section 1734 solely to indicate this fact.

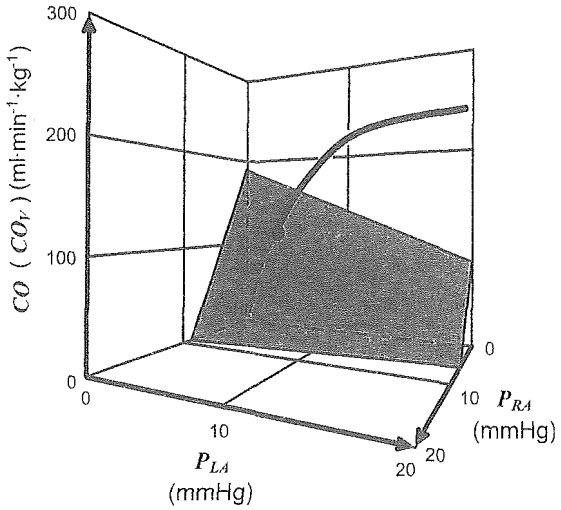

Fig. 1. Diagram of circulatory equilibrium for cardiac output (CO), venous return (CO_V), left atrial pressure (P_{LA}), and right atrial pressure (P_{RA}). Equilibrium CO, P_{LA}, and P_{RA} are obtained as the intersection point of the venous return surface and the integrated CO curve. [Modified from Uemura et al. (29).]

represents the pumping ability of the left or right heart. Therefore, we hypothesized that variations in the CO curve can be explained exclusively by the *S* parameter. Once standard values of the *F* and *H* parameters are determined, we can estimate the integrated CO curve by calculating the *S* parameter from a single set of CO, P_{LA}, and P_{RA} values.

Animal Preparation

We used 15 adult mongrel dogs of either gender (20–30 kg body wt). Care of the animals was in strict accordance with the "Guiding Principles for the Care and Use of Animals in the Field of Physiological Sciences" approved by the Physiological Society of Japan. Anesthesia was induced with pentobarbital sodium (25 mg/kg), and endotracheal intubation was performed. Isoflurane (1.5%) was continuously inhaled to maintain an appropriate level of anesthesia during the experiment. Catheters (6-Fr) were placed in the right femoral artery and vein for withdrawal of blood and for administration of drugs and fluids. To stabilize autonomic tone, we isolated the carotid sinuses bilaterally and maintained the intrasinus pressure constant at 120 mmHg (22). The cervical vagosympathetic trunks were cut. Systemic arterial pressure was measured by a catheter-tipped micromanometer (model PC-751, Millar Instruments, Houston, TX) placed in the ascending aorta via the right carotid artery. After a median sternotomy, a small pericardial incision was made at the level of the aortic root. An ultrasonic flowmeter (model 20A594, Transonics, Ithaca, NY) was placed around the ascending aorta via the incision to measure CO. Fluid-filled catheters were placed in the left and right atria via the incision to measure P_{LA} and P_{RA}, respectively. They were connected to pressure transducers (model DX-200, Nihon Kohden, Tokyo, Japan). The junction between the inferior vena cava and the right atrium was taken as the reference point for zero pressure (22).

Experimental Protocol

Under normal control conditions, we first infused ~250 ml of 10% dextran solution via the right femoral vein. We withdrew blood from the femoral artery in steps of 2 ml/kg to a total volume of 16–22 ml/kg (8–11 steps per animal). In each step, after waiting for 1 min, we recorded CO, P_{LA}, and P_{RA} for ~10 s (Fig. 2). We assumed that this volume reduction alters only the stressed blood volume of the systemic and pulmonary circulation. Because we isolated the baroreceptors, baroreflex-related changes in unstressed blood volume were negligible. We defined the reference values of CO, P_{LA}, and P_{RA} when half of the volume reduction was attained.

To create left ventricular failure, we embolized the left circumflex coronary artery with 90-μm-diameter glass microspheres (28). We adjusted the number of microspheres injected so as to increase P_{LA} by 20 mmHg. We then volume loaded the animals and repeated the protocol described above.

The data were recorded while respiration was temporarily suspended at end expiration. All analog signals were digitized at 200 Hz with a 12-bit analog-to-digital converter (model AD12-16UE, Contec, Osaka, Japan) using a dedicated laboratory computer system (model MA 20V, NEC, Tokyo, Japan) and were stored on a hard disk for subsequent analysis. All the recorded data were averaged over 5 s. All data, except pressure data, were normalized to individual body weight.

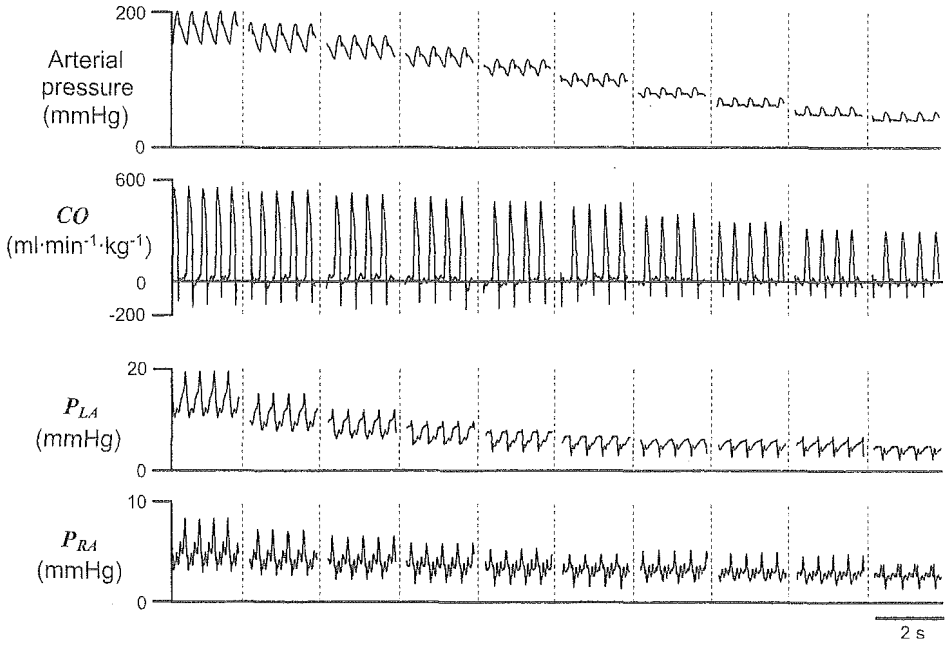

Fig. 2. Changes in arterial pressure, CO, P_{LA}, and P_{RA} throughout the examination. As P_{RA} and P_{LA} decrease after stepwise reduction of the stressed blood volume, CO also decreases (Frank-Starling mechanism).

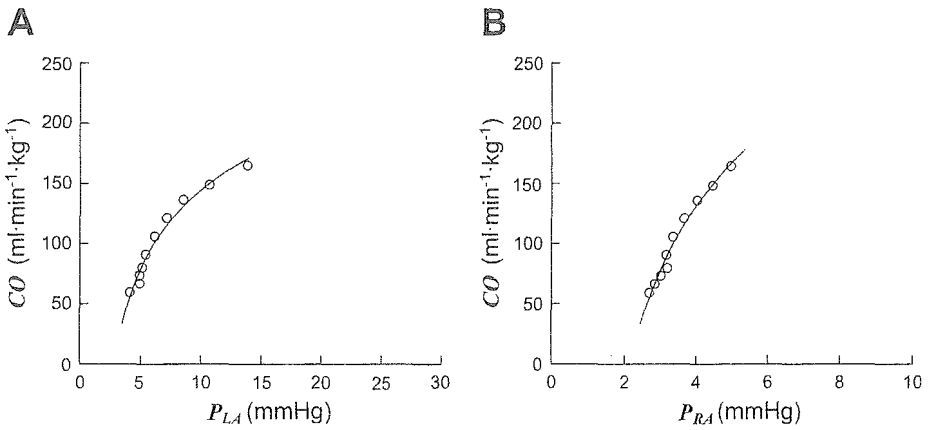

Fig. 3. Relation between CO and P_{LA} (*A*) and between CO and P_{RA} (*B*) in 1 dog. Solid curves, best fit of the 3-parameter logarithmic functions obtained by least-squares method.

Data Analysis

Determination of standard values of F and H parameters. We determined the standard values of the *F* and *H* parameters in seven randomly selected dogs (*group 1*). Using the least-squares method, we fitted the P_{LA}-CO and P_{RA}-CO relations obtained under normal conditions to the three-parameter logarithmic functions (*Eqs. 1* and *2*). We averaged the *F* and *H* values of the left and right heart for the seven animals. The averaged values were used as the standard *F* and *H* parameters in subsequent analyses.

Estimation of the integrated CO curve. Using the standard *F* and *H* parameters, we examined whether we could estimate the integrated CO curve from a single set of CO, P_{LA}, and P_{RA} values. For each animal in *group 1*, we calculated the *S* parameter by substituting the reference values of CO, P_{LA}, and P_{RA} into *Eqs. 1* and *2*. This calculation was done under normal and heart failure conditions. After calculation of the *S* parameter, the P_{LA} and P_{RA} measured in each step were substituted into *Eq. 1* to estimate CO of the left heart and into *Eq. 2* to estimate CO of the right heart. The estimated and measured CO were compared by linear regression analyses.

Prediction of circulatory equilibrium. In the other eight dogs (*group 2*), we estimated the integrated CO curve and venous return surface. The CO curve was estimated as described above using the standard *F* and *H* parameters. Venous return surface was estimated according to our previous work (29) as follows

$$CO_V = V/0.129 - 19.61P_{RA} - 3.49P_{LA} \quad (3)$$

where V is the stressed blood volume, CO_V is the integrated venous return, and 0.129 (min), 19.61 ($ml \cdot min^{-1} \cdot kg^{-1} \cdot mmHg^{-1}$), and 3.49 ($ml \cdot min^{-1} \cdot kg^{-1} \cdot mmHg^{-1}$) are standard parameters characterizing the venous return surface (29). The reference CO, P_{LA}, and P_{RA} values were used to calculate V, which served as the reference stressed volume.

With altered V (from +8 to −8 ml/kg of the reference value), we numerically determined the intersection of the venous return surface (*Eq. 3*) and the integrated CO curve (*Eqs. 1* and *2*) to predict CO, P_{LA}, and P_{RA}. The predicted CO, P_{LA}, and P_{RA} were compared with the measured values. We considered the change in V (±8 ml/kg) to be substantial relative to the physiological stressed blood volume (~25 ml/kg) (17).

Statistics

Group data are expressed as means (SD). The level of statistical significance was defined as $P < 0.05$. To test the goodness of fit, the coefficient of determination (r^2) and the standard error of estimate (SEE) were calculated.

RESULTS

Determination of the Standard Parameters

Figure 3 shows the measured P_{LA}-CO and P_{RA}-CO relations in a representative dog. CO increases in response to increases in P_{LA} or P_{RA} by the Frank-Starling mechanisms. These relations could be fitted to the three-parameter logarithmic function as follows: $CO = 66.7[\ln(P_{LA} - 2.08) + 0.1]$, $r^2 = 0.98$, SEE = 5.9 $ml \cdot min^{-1} \cdot kg^{-1}$ (Fig. 3*A*) and $CO = 112.7[\ln(P_{RA} - 1.39) + 0.19]$, $r^2 = 0.98$, SEE = 5.5 $ml \cdot min^{-1} \cdot kg^{-1}$ (Fig. 3*B*).

Table 1 summarizes the results of the fit in seven dogs. Coefficients of determination were high for the left heart (r^2 = 0.95–0.99) and the right heart (r^2 = 0.90–0.99). These results indicated that the logarithmic functions represented the CO curves of the left and right heart with good accuracy. The averaged *F* and *H* values (F_L = 2.03 mmHg, H_L = 0.80, F_R = 2.13 mmHg, and H_R = 1.90) for seven animals were used as standard values in subsequent analyses.

Table 1. *Fit of CO-P_{LA} and CO-P_{RA} relations to three-parameter logarithmic functions*

Dog	S_L	F_L	H_L	r^2	SEE
1	58.1	1.27	0.61	0.98	4.3
2	24.4	2.03	2.71	0.95	3.6
3	108.4	0.00	−0.67	0.95	5.6
4	66.7	2.08	0.08	0.98	5.9
5	105.6	2.30	−0.02	0.99	5.0
6	73.5	2.21	0.59	0.99	2.5
7	42.0	4.32	2.30	0.98	4.7
Mean (SD)	68.4 (30.9)	2.03 (1.29)	0.80 (1.25)	0.97	4.5 (1.2)
Dog	S_R	F_R	H_R	r^2	SEE
1	46.7	2.12	2.34	0.98	4.7
2	33.9	1.50	2.50	0.96	3.3
3	64.1	2.10	2.10	0.90	8.2
4	112.7	1.39	0.19	0.98	5.5
5	101.8	1.39	0.92	0.99	4.6
6	80.6	3.07	1.59	0.99	2.8
7	37.1	3.33	3.69	0.94	6.8
Mean (SD)	68.1 (31.3)	2.13 (0.8)	1.90 (1.14)	0.96	5.1 (1.9)

S_L and S_R ($ml \cdot min^{-1} \cdot kg^{-1}$), F_L and F_R (mmHg), and H_L and H_R (unitless), parameters of the logarithmic function for left and right hearts, respectively (see METHODS for calculations); r^2, coefficient of determination; SEE, standard error of the estimate ($ml \cdot min^{-1} \cdot kg^{-1}$).

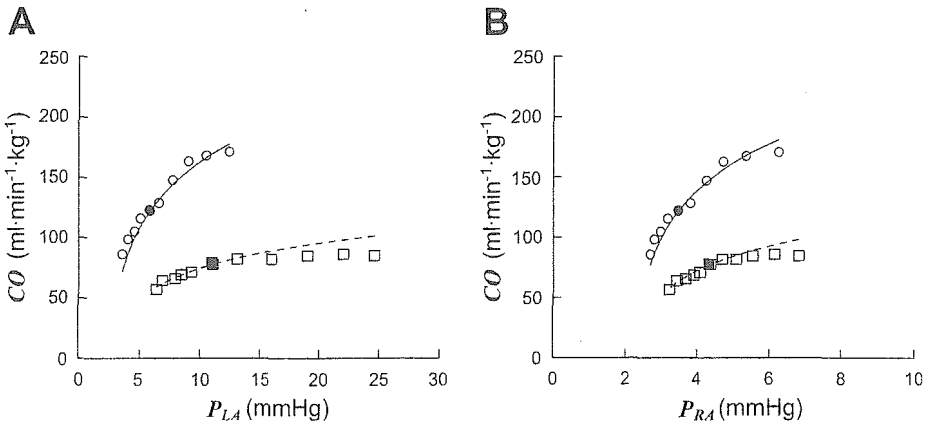

Fig. 4. CO curves for 1 animal under normal conditions and left ventricular failure for the left heart (*A*) and the right heart (*B*). ●, Reference hemodynamic values under normal conditions; ■, reference hemodynamic values under left ventricular failure; ○, measured points under normal conditions; □, measured points under left ventricular failure. Estimated CO curves under normal conditions (solid lines) and under left ventricular failure (dashed lines) accurately correspond with measured points.

Estimation of the Integrated CO Curve

Figure 4 shows the estimated CO curves under normal and heart failure conditions for a single animal. From the reference values, we calculated individual values of the *S* parameter. Under normal conditions, the estimated CO curve accurately coincided with the measured points in the left and the right heart. A good agreement was also observed under left ventricular failure.

Figure 5 demonstrates the relation between estimated and measured CO of pooled data from seven animals (*group 1*). The estimated CO agreed with the measured CO in the left and right heart.

Prediction of Circulatory Equilibrium

Figure 6 illustrates the accuracy of prediction of hemodynamics in response to changes in stressed blood volume (8 dogs, *group 2*). Figure 6*A* shows the relation between predicted and measured CO. CO was predicted accurately over a wide range of CO values from 30 to 200 ml·min^{-1}·kg^{-1}. A small intercept value with a slope near unity also indicates the accuracy of prediction. Figure 6*B* shows the accuracy of the P_{LA} prediction. Although variability increased in the high pressure range (>20 mmHg), the prediction was reasonably accurate. Similarly, P_{RA} was also predicted with reasonable accuracy (Fig. 6*C*).

DISCUSSION

The results of this study indicate that once a single set of steady-state CO, P_{LA}, and P_{RA} values is available, it is possible to predict the changes in hemodynamic variables resulting from a known amount of change in stressed blood volume. This prediction can be very helpful in management of patients under unstable hemodynamic conditions (13, 23).

Estimation of the Integrated CO Curve

We have shown that the integrated CO curve can be estimated with reasonable accuracy under normal and heart failure conditions (Figs. 4 and 5). By fixing the *F* and *H* parameters and by ascribing the changes in the CO curve exclusively to the *S* parameter, we were able to estimate the integrated CO curve from a single set of hemodynamic measurements. As shown in the APPENDIX, the *F* and *H* parameters are mainly related to the end-diastolic pressure-volume relation (*Eq. A4*). In advanced cardiac disorders seen clinically, the end-diastolic pressure-volume relation may vary drastically (6, 7). Hypertensive or idiopathic cardiomyopathy sometimes induces severe ventricular hypertrophy, thereby significantly altering the diastolic ventricular pressure-volume relation (14). In such cases, it may be desirable not to use fixed values but, rather, to estimate *F* and *H* parameters in individual patients. The cardiovascular properties shown in *Eq. A4* can be estimated noninvasively under a steady-state hemodynamic condition (3, 12). Integration of these properties into our method may allow independent estimation of the three parameters in individual patients.

The following validations indicate that our mathematical model of the CO curve and its estimation are consistent with previous investigations. First, on the basis of *Eq. A4* (see

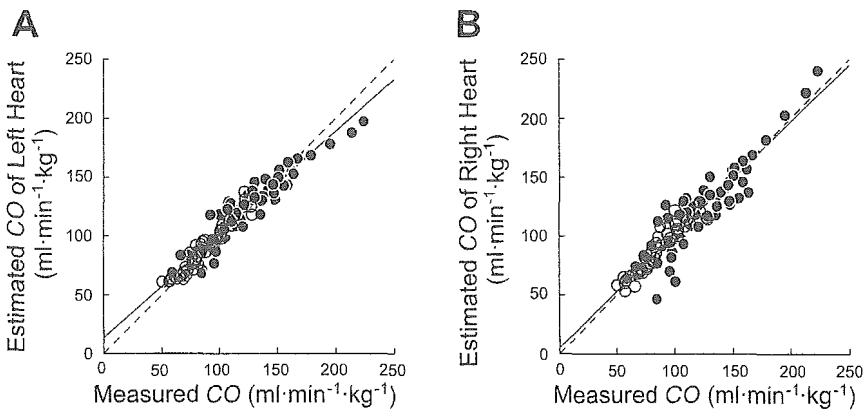

Fig. 5. Relation between estimated and measured values of CO for left heart (*A*) and right heart (*B*) for 104 steps pooled over 13 CO curves. ●, Normal cardiac function; ○, left heart failure; dashed line, line of identity. Regression analysis (solid line) reveals that estimated CO agrees well with measured CO in the left heart [y = 0.88x + 13.3, n = 104, r^2 = 0.93, standard error of estimate (SEE) = 8.7 ml·min^{-1}·kg^{-1}] and right heart (y = 0.96x + 5.0, n = 104, r^2 = 0.88, SEE = 12.1 ml·min^{-1}·kg^{-1}).

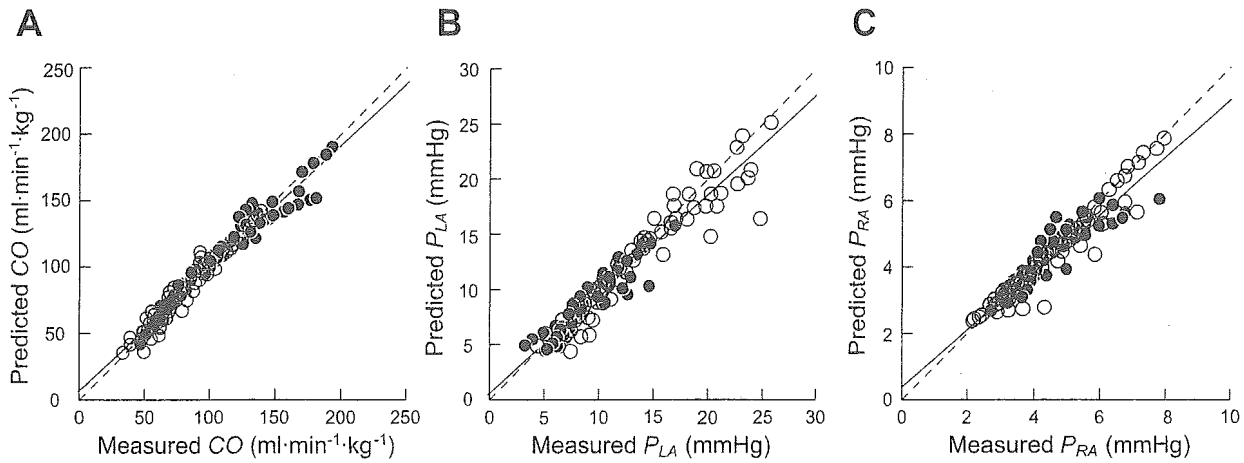

Fig. 6. Relation between predicted and measured values for CO (*A*), P_{LA} (*B*), and P_{RA} (*C*) for 128 steps under normal cardiac function (●) and left heart failure (○). Dashed line, line of identity. Prediction was done by intersecting the venous return surface and the integrated CO curve, both of which were estimated from a set of reference hemodynamic values. Regression analysis (solid line) reveals that predicted CO ($y = 0.93x + 6.5$, $n = 128$, $r^2 = 0.96$, SEE = 7.5 ml·min^{-1}·kg^{-1}), P_{LA} ($y = 0.90x + 0.5$, $n = 128$, $r^2 = 0.93$, SEE = 1.4 mmHg), and P_{RA} ($y = 0.87x + 0.4$, $n = 128$, $r^2 = 0.91$, SEE = 0.4 mmHg) agree reasonably well with measured values.

APPENDIX), using previously reported data (6, 11, 18, 25), we calculated the three parameters in the logarithmic function for the left heart. The values of the cardiovascular properties were chosen to be appropriate for a 20-kg dog (Table 2). The calculated S_L (34 ml·min^{-1}·kg^{-1}), F_L (3.2 mmHg), and H_L (1.14) were compatible with those obtained in our experiment (Table 1). Second, Pouleur et al. (19) examined the CO curve of the left heart in dogs under various cardiac conditions (control, coronary occlusion, and nitroprusside infusion under control and coronary occlusion). Their CO curves could be approximated to our three-parameter logarithmic functions with reasonable accuracy ($r^2 = 0.94–0.99$). When we applied the standard values of F_L (2.03 mmHg) and H_L (0.80) obtained in this study to their data and estimated their CO curve, the estimated CO closely correlated with the values measured ($y = 0.67x + 29.0$, $r^2 = 0.90$, SEE = 5.0 ml·min^{-1}·kg^{-1}, from 40 to 150 ml·min^{-1}·kg^{-1}).

Clinical Application of the Framework of Circulatory Equilibrium

Cardiac patients frequently receive empirical fluid challenges to treat low CO, unexplained hypotension, and oliguria (1, 32). Such empirical challenges sometimes exert deleterious effects by excessive volume expansion (1, 32). Our framework is free of such problems, because we can accurately estimate the stressed blood volume of the patient and predict hemodynamics resulting from the volume challenge, once we measure a single set of steady-state CO, P_{LA}, and P_{RA} values with, for example, Swan-Ganz catheters (2).

Table 2. *Values of the cardiovascular properties from previously reported data*

Parameter	Value
HR, beats/min	120
T, min	0.0083
R, mmHg·min·ml^{-1}	0.031
E_{es}, mmHg/ml	10
V_0, ml	5
k, ml^{-1}	0.13
α, mmHg	0.25
β, mmHg	4.8
γ (unitless)	1.5

HR, heart rate; T, heart period; R, systemic arterial resistance; E_{es}, end-systolic elastance of left ventricle; V_0, volume at which end-systolic pressure is 0 mmHg in the left ventricle; k, α, and β, constants characterizing end-diastolic pressure-volume relation of the left ventricle; γ, ratio of left ventricular end-diastolic pressure to mean left atrial pressure.

The outcome of acute or chronic heart failure has been related to the severity of reduced CO and elevated left ventricular filling pressure (4, 5, 13, 23). Several studies, however, indicate that patients with Forrester class IV hemodynamics are not necessarily condemned to a class IV prognosis. Even if the initial hemodynamics are classified as class IV, patients showing reduction in filling pressure after intensive medical therapy have a better prognosis than those without reduction in filling pressure (13, 23). With use of our framework for guidance, proper management of low CO and elevated filling pressures would improve the prognosis of such patients.

In clinical settings, the reference point for zero pressure is determined by an empirical external inspection (16). Changes in the patient's position relative to the pressure transducer may induce apparent changes in atrial pressures (16). These factors can result in a measurement error for atrial pressure and, consequently, an error in the prediction of the circulatory equilibrium. Accurate determination of the external reference point relative to the level of the right atrium and strict attention to patient position are required for clinical application of our framework.

Limitations of the Study

All the experiments of this study were conducted in anesthetized, open-chest dogs. Anesthesia and surgical trauma significantly affect the cardiovascular system (31). Whether this equilibrium framework can be applied to conscious, closed-chest animals (including humans) remains to be tested.

25. **Suga H and Sagawa K.** Instantaneous pressure-volume relationships and their ratio in the excised, supported canine left ventricle. *Circ Res* 35: 117–126, 1974.
26. **Sunagawa K, Maughan WL, Burkhoff D, and Sagawa K.** Left ventricular interaction with arterial load studied in isolated canine ventricle. *Am J Physiol Heart Circ Physiol* 245: H773–H780, 1983.
27. **Sunagawa K, Sagawa K, and Maughan WL.** Ventricular interaction with the loading system. *Ann Biomed Eng* 12: 163–189, 1984.
28. **Todaka K, Leibowitz D, Homma S, Fisher PE, Derosa C, Stennett R, Packer M, and Burkhoff D.** Characterizing ventricular mechanics and energetics following repeated coronary microembolization. *Am J Physiol Heart Circ Physiol* 272: H186–H194, 1997.
29. **Uemura K, Sugimachi M, Kawada T, Kamiya A, Jin Y, Kashihara K, and Sunagawa K.** A novel framework of circulatory equilibrium. *Am J Physiol Heart Circ Physiol* 286: H2376–H2385, 2004.
30. **Ursino M.** Interaction between carotid baroregulation and the pulsating heart: a mathematical model. *Am J Physiol Heart Circ Physiol* 275: H1733–H1747, 1998.
31. **Vatner SF and Braunwald E.** Cardiovascular control mechanisms in the conscious state. *N Engl J Med* 293: 970–976, 1975.
32. **Wagner JG and Leatherman JW.** Right ventricular end-diastolic volume as a predictor of the hemodynamic response to a fluid challenge. *Chest* 113: 1048–1054, 1998.

We isolated baroreceptors and fixed the autonomic tone in this study. This was necessary, because the baroreflex alters the CO curve and venous return surface through its effects on stressed blood volume, vascular resistance, heart rate, and cardiac contractility (8, 22). How changes in autonomic tone under the closed-loop condition affect the accuracy of hemodynamic prediction remains to be investigated.

Conclusion

The integrated CO curve can be estimated on the basis of a single set of hemodynamic measurements (CO, P_{LA}, and P_{RA}). The integrated CO curve thus estimated enables accurate prediction of hemodynamics (CO, P_{LA}, and P_{RA}) after extensive changes in stressed blood volume during heart failure and normal cardiac function.

APPENDIX

Mathematical modeling of the CO curve. We derived the relation between CO and atrial pressure on the basis of the ventricular pressure-volume relation framework (15, 25) and the ventricular-arterial coupling framework (26) as follows.

The relation between the stroke volume (SV) and the ventricular end-diastolic volume (V_{ed}) has been approximated with reasonable accuracy as

$$SV = \frac{TE_{es}}{TE_{es} + R} \times (V_{ed} - V_0) \qquad (A1)$$

where E_{es} is the slope (elastance), V_0 is the volume axis intercept of the ventricular end-systolic pressure-volume relation, T is the heart period, and R is the arterial resistance (20, 25, 26). Dividing SV by T, CO can be expressed as

$$CO = \frac{E_{es}}{TE_{es} + R} \times (V_{ed} - V_0) \qquad (A2)$$

V_{ed} can be interrelated with end-diastolic pressure (P_{ed}) by

$$P_{ed} = \alpha e^{kV_{ed}} + \beta \qquad (A3)$$

where k, α, and β are constants (6, 7). If we approximate P_{ed} by a scaled mean atrial pressure (P_{At}), γP_{At} (γ is a proportionality constant), *Eq. A2* can be rewritten as

$$CO = \frac{1}{k} \cdot \frac{E_{es}}{TE_{es} + R} \times \left[\ln \left(P_{At} - \frac{\beta}{\gamma} \right) + \ln \left(\frac{\gamma}{\alpha} \right) - kV_0 \right] \qquad (A4)$$

which can be simplified by lumping parameters for cardiovascular system properties into three constants, S, F, and H

$$CO = S \times [\ln (P_{At} - F) + H] \qquad (A5)$$

GRANTS

This study was supported by Health and Labor Sciences Research Grants for research on medical devices for analyzing, supporting, and substituting the function of the human body and research on advanced medical technology from the Ministry of Health, Labour, and Welfare of Japan, Japan Society for the Promotion of Science Grants-in-Aid for Scientific Research A 15200040, C 14570707, and C 15590786, and Ministry of Education, Culture, Sports, Science, and Technology Grant-in-Aid for Young Scientists (B) 16700379, as well as the Program for Promotion of Fundamental Studies in Health Science of Pharmaceuticals and Medical Devices Agency of Japan.

REFERENCES

1. **Bendjelid K, Suter PM, and Romand JA.** The respiratory change in preejection period: a new method to predict fluid responsiveness. *J Appl Physiol* 96: 337–342, 2004.
2. **Chaliki HP, Hurrell DG, Nishimura RA, Reinke RA, and Appleton CP.** Pulmonary venous pressure: relationship to pulmonary artery, pulmonary wedge, and left atrial pressure in normal, lightly sedated dogs. *Catheter Cardiovasc Interv* 56: 432–438, 2002.
3. **Chen CH, Fetics B, Nevo E, Rochitte CE, Chiou KR, Ding PA, Kawaguchi M, and Kass DA.** Noninvasive single-beat determination of left ventricular end-systolic elastance in humans. *J Am Coll Cardiol* 38: 2028–2034, 2001.
4. **Crexells C, Chatterjee K, Forrester JS, Dikshit K, and Swan HJ.** Optimal level of filling pressure in the left side of the heart in acute myocardial infarction. *N Engl J Med* 289: 1263–1266, 1973.
5. **Forrester JS, Diamond G, Chatterjee K, and Swan HJG.** Medical therapy of acute myocardial infarction by application of hemodynamic subsets. *N Engl J Med* 295: 1356–1362, 1976.
6. **Glantz SA and Kernoff RS.** Muscle stiffness determined from canine left ventricular pressure-volume curves. *Circ Res* 37: 787–794, 1975.
7. **Glantz SA and Parmley WW.** Factors which affect the diastolic pressure-volume curve. *Circ Res* 42: 171–180, 1978.
8. **Greene AS and Shoukas AA.** Changes in canine cardiac function and venous return curves by the carotid baroreflex. *Am J Physiol Heart Circ Physiol* 251: H288–H296, 1986.
9. **Guyton AC.** Determination of cardiac output by equating venous return curves with cardiac response curves. *Physiol Rev* 35: 123–129, 1955.
10. **Guyton AC, Jones CE, and Coleman TG.** *Circulatory Physiology: Cardiac Output and Its Regulation* (2nd ed.). Philadelphia, PA: Saunders, 1973, p. 263–284.
11. **Lee RW and Goldman S.** Mechanism for decrease in cardiac output with atrial natriuretic peptide in dogs. *Am J Physiol Heart Circ Physiol* 256: H760–H765, 1989.
12. **Little WC, Ohno M, Kitzman DW, Thomas JD, and Cheng CP.** Determination of left ventricular chamber stiffness from the time for deceleration of early left ventricular filling. *Circulation* 92: 1933–1939, 1995.
13. **Lucas C, Johnson W, Hamilton MA, Fonarow GC, Woo MA, Flavell CM, Creaser JA, and Stevenson LW.** Freedom from congestion predicts good survival despite previous class IV symptoms of heart failure. *Am Heart J* 140: 840–847, 2000.
14. **Mandinov L, Eberli FR, Seiler C, and Hess OM.** Diastolic heart failure. *Cardiovasc Res* 45: 813–825, 2000.
15. **Maughan WL, Shoukas AA, Sagawa K, and Weisfeldt ML.** Instantaneous pressure-volume relationship of the canine right ventricle. *Circ Res* 44: 309–315, 1979.
16. **McGee SR.** Physical examination of venous pressure: a critical review. *Am Heart J* 136: 10–18, 1998.
17. **Ogilvie RI and Zborowska-Sluis D.** Effect of chronic rapid ventricular pacing on total vascular capacitance. *Circulation* 85: 1524–1530, 1992.
18. **Ohno M, Cheng CP, and Little WC.** Mechanism of altered patterns of left ventricular filling during the development of congestive heart failure. *Circulation* 89: 2241–2250, 1994.
19. **Pouleur H, Covell JW, and Ross J Jr.** Effects of nitroprusside on venous return and central blood volume in the absence and presence of acute heart failure. *Circulation* 61: 328–337, 1980.
20. **Sagawa K, Maughan WL, Suga H, and Sunagawa K.** *Cardiac Contraction and Pressure-Volume Relationship.* Oxford, UK: Oxford Univ. Press, 1988, p. 232–298.
21. **Sarnoff SJ and Berglund E.** Ventricular function. 1. Starling's law of the heart, studied by means of simultaneous right and left ventricular function curves in the dog. *Circulation* 9: 706–718, 1953.
22. **Shoukas AA.** Carotid sinus baroreceptor reflex control and epinephrine. Influence on capacitive and resistive properties of the total pulmonary vascular bed of the dog. *Circ Res* 51: 95–101, 1982.
23. **Stevenson LW, Tillisch JH, Hamilton M, Luu M, Chelimsky-Fallick C, Moriguchi J, Kobashigawa J, and Walden J.** Importance of hemodynamic response to therapy in predicting survival with ejection fraction less than or equal to 20% secondary to ischemic or nonischemic dilated cardiomyopathy. *Am J Cardiol* 66: 1348–1354, 1990.
24. **Stone HL, Bishop VS, and Dong EJ.** Ventricular function in cardiac denervated and cardiac sympathectomized conscious dogs. *Circ Res* 20: 587–593, 1967.